



HAL
open science

Constitutive equations for coupled flows in clay materials

André Revil, W. F. Woodruff, N. Lu

► **To cite this version:**

André Revil, W. F. Woodruff, N. Lu. Constitutive equations for coupled flows in clay materials. Water Resources Research, 2011, 47, pp.W05548. 10.1029/2010WR010002 . insu-00681416

HAL Id: insu-00681416

<https://insu.hal.science/insu-00681416>

Submitted on 2 Mar 2021

HAL is a multi-disciplinary open access archive for the deposit and dissemination of scientific research documents, whether they are published or not. The documents may come from teaching and research institutions in France or abroad, or from public or private research centers.

L'archive ouverte pluridisciplinaire **HAL**, est destinée au dépôt et à la diffusion de documents scientifiques de niveau recherche, publiés ou non, émanant des établissements d'enseignement et de recherche français ou étrangers, des laboratoires publics ou privés.

Constitutive equations for coupled flows in clay materials

A. Revil,^{1,2} W. F. Woodruff,¹ and N. Lu³

Received 12 September 2010; revised 23 February 2011; accepted 10 March 2011; published 28 May 2011.

[1] We first upscale the local transport (Stokes and Nernst-Planck) equations to the scale of a single capillary saturated by a binary 1:1 electrolyte. These equations are then upscaled to the scale of a network of tortuous capillaries embedded in a homogeneous and continuous mineral matrix, including the influence of the distribution of pore sizes but excluding the effect of connectivity between the pores. One of the features of our theory is to account for transport along the mineral surface in the so-called Stern layer because of recent evidence that this mechanism is effective in describing frequency-dependent electrical conductivity. Real clay materials are, however, not described by a set of capillaries, so we have to modify the model to include the effect of transversal dispersivity, for example. We found no evidence for transport in the Stern layer because of the discontinuity of the solid phase at the scale of a representative elementary volume in clay materials. The effect of the diffuse layer is accounted for through the use of a Donnan equilibrium approach to determine the effective concentrations of the ions in the pore space, which are different from the ionic concentrations of an ionic reservoir in local equilibrium with the porous material. We found that the diffuse layer controls various transport properties, including, for example, the DC electrical conductivity, the osmotic efficiency coefficient, the streaming potential coupling coefficient, and the macroscopic Hittorf numbers. Comparison to a large data set of experimental data, mainly on clay materials, confirms the validity of the derived relationships used to describe the material properties entering into the constitutive equations.

Citation: Revil, A., W. F. Woodruff, and N. Lu (2011), Constitutive equations for coupled flows in clay materials, *Water Resour. Res.*, 47, W05548, doi:10.1029/2010WR010002.

1. Introduction

[2] The development of a set of complete constitutive equations describing the transport of ions and water in a porous material is crucial to interpret some geophysical measurements, including time-lapse self-potential signals [Revil and Jardani, 2010a; Revil et al., 2010], DC resistivity data [Kemna et al., 2000; Knight et al., 2010], electroseismic signals [Pride, 1994; Revil and Jardani, 2010b; Jardani et al., 2010], and induced polarization measurements [Binley et al., 2005; Revil and Florsch, 2010; Vaudelet et al., 2011]. These constitutive equations are also important to connect these geoelectrical measurements to reactive transport modeling codes used to model the transport of contaminants in reactive porous media [Kemna et al., 2000; Snieder et al., 2007; Revil and Jardani, 2010a]. The development of rigorous constitutive equations is also important to understand the role of osmotic processes in sedimentary basins [Fritz, 1986; Jougnot et al., 2009; Neuzil and Provost, 2009] and to model the transport properties of clay-rich materials used as potential hosts

for the long-term storage of nuclear wastes [Sammartino et al., 2003; Delay and Distinguin, 2004; Rousseau-Gueutin et al., 2010].

[3] There are several methods to obtain these macroscopic constitutive equations at the scale of a representative elementary volume of a porous material. Nonequilibrium thermodynamics offers, for instance, a macroscopic framework in the vicinity of thermodynamic equilibrium [e.g., Prigogine, 1947; Olsen, 1960; de Groot and Mazur, 1984; Gray and Hassanizadeh, 1991; Mitchell, 1993; Bennethum and Cushman, 2002a, 2002b; Malusis and Shackelford, 2004; Revil, 2007]. However, such a phenomenological approach is not able to provide relationships between the material properties entering the constitutive equations and (1) the fundamental textural parameters describing the texture of the porous material and (2) the electrochemical properties of the interfaces between the different phases of the porous composite. The development of relationships between the material properties and the texture can be obtained only if upscaling approaches are used, starting with the local equations valid in each phase of the porous material, using appropriate microscopic boundary conditions at the interfaces between phases plus macroscopic boundary conditions at the boundary of the porous material [Dormieux, 2005]. Upscaling methods include, for instance, the volume-averaging method [Whitaker, 1967; Nguyen et al., 1982; Pride, 1994], the homogenization method [Sanchez-Palencia, 1980; Auriault and Lewandowska, 1993], and the differential effective medium approach (see a recent review by Cosenza et al. [2009]).

¹Department of Geophysics, Colorado School of Mines, Golden, Colorado, USA.

²ISTerre, UMR 5559, CNRS, Université de Savoie, Le Bourget du Lac, France.

³Division of Engineering, Colorado School of Mines, Golden, Colorado, USA.

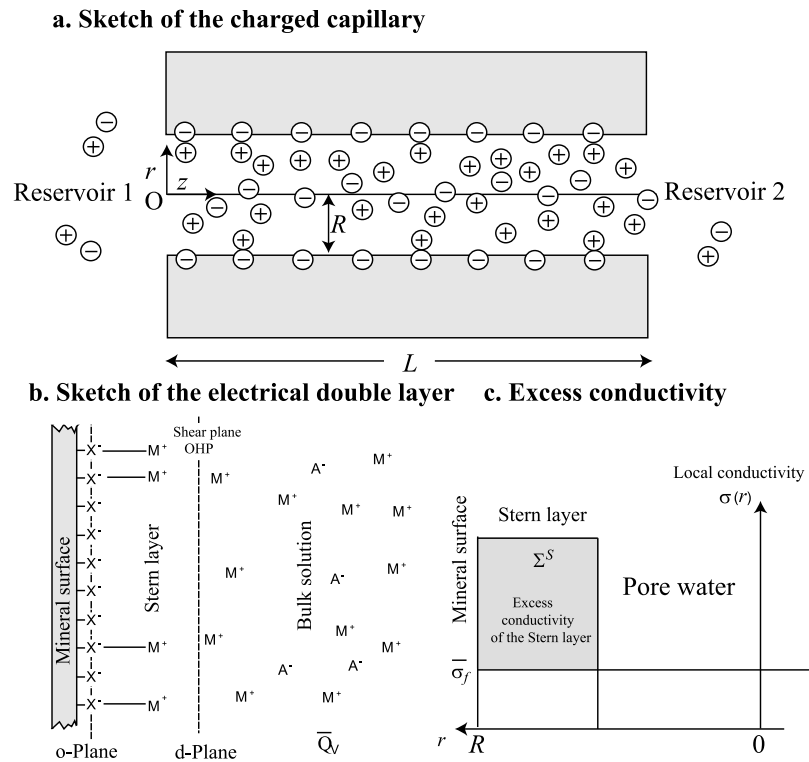


Figure 1. Description of the charged capillary. (a) Sketch of a cylindrical micropore separating two reservoirs of ions at two distinct pressures, salinities, and electrical potentials. The electrolytes in the two reservoirs are the same binary symmetric electrolytes. The model corresponds to the thick double-layer assumption; for example, there is no neutral pore water. (b) Sketch of the electrical double layer. The double layer comprises a layer of counterions sorbed onto the mineral surface and a diffuse layer with Coulombic interaction only. (c) Sketch of the electrical conductivity distribution showing the excess surface conductivity Σ_S (in S) of the Stern layer and the effective conductivity of the pore water $\bar{\sigma}_f$ with an excess of counterions from the diffuse layer. The position $r = 0$ corresponds to the centerline of the capillary, while the position $r = R$ characterizes the interface between the solid and fluid phases.

[4] In the present paper, we are interested in developing a simple and practical model for the coupled constitutive equations (coupled flows) in a saturated clay material. Our model is explicitly valid for clay media, but we believe that the theory would work to a good approximation for other types of porous materials. We start our modeling effort considering that the pore space can be approximated by a set of nonconnected capillaries [e.g., Pfannkuch, 1972; Dullien, 1992; Jackson, 2008, 2010; Linde, 2009, and references therein]. The effect of connectivity and discontinuity of the solid phase will be, however, accounted for later. Transport along the mineral surface in the Stern layer seems to be a missing component in transport models, despite the increasing body of evidence that such a transport mechanism is important in describing the frequency-dependent electrical conductivity of rocks [Zukoski and Saville, 1986a, 1986b; Leroy et al., 2008; Leroy and Revil, 2009; Revil and Florsch, 2010]. While the present paper is dedicated only to the saturated and isothermal case (see Leinov et al. [2010] for a recent application to the nonisothermal case), we consider our model to be a first step in achieving a complete theory for the unsaturated case in clay materials. In this case, the relationship between the capillary pressure curve and the pore size distribution should account for the different types of waters present in the pore space, especially the hydration

and capillary waters. As pointed out, the present approach could also be an important step forward in connecting geophysical methods to reactive transport modeling. The pore size distribution can be obtained independently, for example, from nuclear magnetic resonance (NMR) relaxometry data [Stingaciu et al., 2010]. Because the contribution of the Stern layer is incorporated, the model could be applied at the grain scale to provide a unified model of low-frequency induced polarization, including the Stern layer polarization, the membrane polarization, and the Maxwell-Wagner polarization. Such unification of polarization effects has not been realized to date.

2. Constitutive Equations

[5] We develop below a complete set of constitutive equations for a clay material with the pore space modeled as a set of nonconnecting charged capillaries (Figure 1). We first explore the case for which all the capillaries have the same radius R and then the case for which the capillaries are modeled with a pore size distribution described by a (normalized) probability density function $g(R)$. In both cases, we are not concerned with nanopores, for which the finite size of the ions needs to be taken into account [Cervera et al., 2010] and for which activity must be used in the definition

Table 1. Nomenclature of the Material Properties

Symbol	Definition	Units
F	Formation factor	dimensionless
m	Cementation exponent	dimensionless
ϕ	Connected porosity	dimensionless
k	Permeability	m^2
k_c	Osmotic permeability	m^2
σ	Electrical conductivity	S m^{-1}
$\sigma_{(\pm)}$	Ionic contribution to the electrical conductivity	S m^{-1}
$T_{(\pm)}$	Macroscopic Hittorf numbers	dimensionless
CEC	Cation exchange capacity	C kg^{-1}
R	Pore radius (capillary)	m
Λ	Effective pore radius (porous material)	m
α_L	Longitudinal dispersivity	m
α_T	Transverse dispersivity	m
n	Number of capillaries	dimensionless
Q_S	Effective surface charge density of the minerals	C m^{-2}
Q_0	True surface charge density of the minerals	C m^{-2}
Q_β	Surface charge density of the Stern layer	C m^{-2}
\bar{Q}_V	Volumetric charge density in the pore space	C m^{-3}
A	Surface area of a cross section of porous material	m^2
S	Pore water-mineral surface area	m^2
V_p	Pore volume	m^3
ε	Osmotic efficiency	dimensionless
D	Effective diffusion coefficient	$\text{m}^2 \text{s}^{-1}$
C	Streaming potential coupling coefficient	V Pa^{-1}
ϕ	Connected porosity	dimensionless
$\underline{\underline{\mathbf{M}}}$	Matrix of material properties	NA
$\underline{\underline{\mathbf{D}}}$	Dispersivity tensor	NA
Θ	Dimensionless charge density of the diffuse layer	dimensionless
Ψ	Dimensionless charge density of the Stern layer	dimensionless

of the chemical potential, rather than concentrations. Therefore, the theory we use will be valid mainly for micropores (pore size on the order of the thickness of the Debye length, typically $<0.2 \mu\text{m}$; see Figure 1), a valid assumption when working with clay materials.

[6] The sequence for upscaling the local equations is as follows: (1) identify the form of the constitutive equations at the microscale (including potential transport in the Stern layer and the osmotic pressure) and determine the correct microboundary and macroboundary conditions, (2) average over a single capillary, and (3) average over a set of capillaries to obtain the constitutive equations for the flux densities, accounting for the pore size distribution using the raw moments of the pore size distribution. The different parameters used in our model are defined in Tables 1–3.

2.1. Upscaling Using a Single Capillary

[7] We consider a capillary of radius R and length L ($\gg R$ to avoid edge effects) saturated by a binary symmetric 1:1 electrolyte like NaCl or KCl. We use polar coordinates with r as the radial coordinate in the plane normal to the capillary and z in the direction along the capillary. The capillary is in contact with two neutral reservoirs of ions, one upstream at $z = 0$ (reservoir 1) and one downstream at $z = L$ (reservoir 2; see Figure 1a). The macroscopic potentials controlling transport phenomena in the capillary are controlled by the differ-

ence of potential between these two macroscopic reservoirs. In the case where there are no such reservoirs, a fictitious reservoir locally in equilibrium with the porous material should be considered.

[8] We consider that the surface of the capillary is negatively charged. The opposite case of a positively charged mineral surface is just the symmetric case of the one considered below. The present model could also be easily coupled to electrical double-layer theory, as explained below. The negative surface charge density Q_S includes the true mineral surface charge density Q_0 plus the surface charge density of the Stern layer of adsorbed counterions Q_β [Leroy et al., 2007] (Figures 1b and 1c). In theory, Q_S may depend slightly on the capillary size because of the overlapping of the electrical double layer and the difference in salinity in the different capillaries [Gonçalvès et al., 2007; Wang and Revil, 2010]. In the present approach, we will consider that this dependence is so small that it can be safely neglected. The charge density \bar{q}_V (>0 , in C m^{-3}) denotes the volumetric charge density in the capillary (the pore water is therefore not neutral). The local electroneutrality equation of the capillary, as a whole, is therefore

$$\bar{q}_V + Q_S \frac{S}{V_p} = 0, \quad (1)$$

where $S = 2\pi RL$ is the internal surface of the capillary and $V_p = \pi R^2 L$ represents its volume.

[9] We use the Teorell-Meyer-Sievers (TMS) model (also called the Donnan model in the literature [see Teorell, 1935;

Table 2. Nomenclature of the Potentials, Concentrations, Pressures, Fluxes, and Forces

Symbol	Definition	Unit
ψ	Electrostatic potential in the reservoirs	V
$\bar{\varphi}$	Electrostatic potential in the pore water due to the diffuse layer	V
\mathbf{E}	Electrical field	V m^{-1}
\mathbf{v}	Mean velocity of the pore water	m s^{-1}
$\bar{\varphi}$	Mean electrostatic potential in the pores	V
$\bar{\pi}$	Osmotic pressure in the pore space	Pa
π	Osmotic pressure in the reservoirs	Pa
$\tilde{\mu}_{(\pm)}$	Electrochemical potential of the ions in the pore space	J
$\tilde{\mu}_{(\pm)}$	Electrochemical potential of the ions in the reservoirs	J
$\mu_{(\pm)}^0$	Standard chemical potential of the ions	J
$\tilde{\mu}_{(\pm)}^S$	Electrochemical potential of the ions along the Stern layer	J
μ_w	Chemical potential of water in the reservoirs	J
μ_w^0	Chemical potential of water in the reference state	J
p	Reservoir mechanical fluid pressure	Pa
p^*	Reservoir total fluid pressure	Pa
\bar{p}	Pore fluid pressure	Pa
\mathbf{J}_d	Macroscopic flux density of the salt	$\text{mol m}^{-2} \text{s}^{-1}$
$\mathbf{J}_{(\pm)}$	Macroscopic flux density of the ions	$\text{mol m}^{-2} \text{s}^{-1}$
\mathbf{U}	Macroscopic Darcy velocity	m s^{-1}
\mathbf{J}	Macroscopic current density	A m^{-2}
\mathbf{F}	External body force applied to the pore water	N m^{-3}
$\mathbf{j}_{(\pm)}$	Local flux of cations and anions	$\text{mol m}^{-2} \text{s}^{-1}$

Table 3. Nomenclature of the Other Parameters and Constants

Symbol	Definition	Unit
T	Temperature	K
L	Distance between the reservoirs	L
$K_{(\pm)}$	Sorption constants on the mineral surface	$\text{m}^3 \text{mol}^{-1}$
$\bar{\sigma}_f$	Conductivity of the pore water	S m^{-1}
σ_f	Conductivity of the water in the reservoirs	S m^{-1}
D_f	Diffusion coefficient of the salt in the reservoirs	$\text{m}^2 \text{s}^{-1}$
$t_{(\pm)}$	Microscopic Hittorf numbers	dimensionless
$b_{(\pm)}$	Diffusional mobility of the ions in the pore water	$\text{m}^2 \text{s}^{-1} \text{J}^{-1}$
$\beta_{(\pm)}$	Electromigration mobilities of the ions in the pore water	$\text{m}^2 \text{s}^{-1} \text{V}^{-1}$
$b_{(\pm)}^S$	Diffusional mobility of the ions in the Stern layer	$\text{m}^2 \text{s}^{-1} \text{J}^{-1}$
$\beta_{(\pm)}^S$	Electromigration mobilities of the ions in the Stern layer	$\text{m}^2 \text{s}^{-1} \text{V}^{-1}$
ρ_g	Mass density of the grains	kg m^{-3}
ρ_f	Mass density of the pore water	kg m^{-3}
$C_{(\pm)}$	Concentration of the ions in the reservoirs	mol m^{-3}
$\bar{C}_{(\pm)}$	Concentration of the ions in a single capillary	mol m^{-3}
$\bar{C}_{(\pm)}$	Concentration of the ions in the pore space	mol m^{-3}
C_f	Salinity in the reservoir	mol m^{-3}
Π_n	Raw moment of order n of the pore size distribution	m^n
e	Elementary charge of the electron	C
k_b	Boltzmann constant	J K^{-1}
$\Gamma_{(+)}$	Surface density of $>\text{SO}^-\text{M}^+$ surface sites	m^{-2}
$\Gamma_{(-)}$	Surface density of $>\text{SOH}_2\text{A}^-$ surface sites	m^{-2}
$\Gamma_{(-)}^0$	Surface density of $>\text{SO}^-$ surface sites	m^{-2}
$\Gamma_{(+)}^0$	Surface density of $>\text{SOH}_2^+$ surface sites	m^{-2}
Ω_w	Molecular volume of water	$\text{m}^3 \text{mol}^{-1}$

Meyer and Sievers, 1936]) to describe the mean concentrations in the pore space of the capillary (see Appendix A). This approximation is used to avoid involving the more rigorous solution of the Poisson-Boltzmann equation [Pride, 1994; Furini et al., 2006]. As demonstrated by Westermann-Clark and Christoforou [1986], the use of the TMS approach is valid in the case where the thickness of the diffuse layer is on the same order of magnitude as the size of the pores. If we consider clay materials, this assumption is therefore valid. Usually, it is also a good assumption even for macropores, but validation of this would require a complete analysis that is outside the scope of the present paper.

[10] From equation (1), the relationship between the volumetric charge density and the surface charge density Q_s (which is constant for all capillaries) is

$$\bar{q}_V = -Q_s \frac{S}{V_p} = -Q_s \frac{2}{R}. \quad (2)$$

Therefore, \bar{q}_V is inversely proportional to the pore radius.

[11] Pride [1994], Furini et al. [2006], and Westermann-Clark and Christoforou [1986] used the Stokes equation for the pore water without accounting for the presence of the ions, except in the body force, thereby neglecting the osmotic pressure in the constitutive equations. In our approach, we come back to a more fundamental Stokes equation in which the pore water is a mixture of water molecules and ions. The Stokes

equation for the transport of the salty water in a capillary should, therefore, be written in term of differences (or gradients) in the chemical potentials between the two reservoirs. This yields

$$-\bar{c}_w \nabla \mu_w - \bar{c}_{(+)} \nabla \mu_{(+)} - \bar{c}_{(-)} \nabla \mu_{(-)} + \mathbf{F} + \eta \nabla^2 \mathbf{v} = 0, \quad (3)$$

$$-\bar{c}_w \Omega_w \nabla (p - \pi) - \bar{c}_{(+)} \nabla \mu_{(+)} - \bar{c}_{(-)} \nabla \mu_{(-)} + \mathbf{F} + \eta \nabla^2 \mathbf{v} = 0, \quad (4)$$

$$-\nabla (p - \pi) + \eta \nabla^2 \mathbf{v} + \mathbf{F} - \bar{c}_{(+)} \nabla \mu_{(+)} - \bar{c}_{(-)} \nabla \mu_{(-)} = 0, \quad (5)$$

as $\bar{c}_w \Omega_w \approx 1$, where \bar{c}_w is the concentration of water molecules per unit volume of the pore fluid in the capillary, Ω_w represents the molecular volume of water (in $\text{m}^3 \text{molecule}^{-1}$), p is the mechanical pore water pressure (in Pa, not related to concentrations), π is the osmotic pressure (see Appendix A), η is the dynamic viscosity of the pore water (in Pa s), \mathbf{v} is the velocity of the pore fluid in the capillary (in m s^{-1}), \mathbf{F} is the external body force applied to the pore fluid (in N m^{-3}), $\bar{c}_{(\pm)}$ are the average concentrations of the cations and anions in the capillary, and $\mu_{(\pm)} = \mu_{(\pm)}^0 + k_b T \ln C_{(\pm)}$ are the macroscopic chemical potentials of the cations and anions in the reservoirs (in J), where k_b is the Boltzmann constant ($1.381 \times 10^{-23} \text{ J K}^{-1}$), T is the absolute temperature (in K), $\mu_{(\pm)}^0$ is the chemical potential in a reference state, and $C_{(\pm)}$ are the macroscopic concentrations in the reservoirs in contact with the capillary (in m^{-3}). In equation (5), the pressure difference $p^* = p - \pi$ represents the total water potential in the reservoirs, omitting the gravitational term if this term is accounted for in the body force. There is a gradient in the osmotic pressure between the two reservoirs because of the salinity gradient between the two reservoirs.

[12] The macroscopic boundary conditions for the hydrodynamic fluid pressure are

$$p = p_1, \quad z = 0, \quad (6)$$

$$p = p_1 - \delta p, \quad z = L, \quad (7)$$

in reservoirs 1 and 2, respectively, with $\delta p > 0$. The unit vector \hat{z} is in the flow direction. Neglecting gravity (or, alternatively, keeping the gravity in the total hydraulic head), the body force entering equation (3) is given by the Coulomb force,

$$\mathbf{F} = \bar{q}_V \mathbf{E}, \quad (8)$$

where \mathbf{E} is the external electrical field (in V m^{-1}). In the quasi-static limit of the Maxwell equations (no electromagnetic induction), we have $\nabla \times \mathbf{E} = 0$, and therefore, the electrical field can be derived from the gradient of a scalar potential,

$$\mathbf{E} = -\nabla \psi, \quad (9)$$

where ψ is the electrical potential (in V; electromotive potential) defined in the two reservoirs (only the difference of potential is measurable). The boundary conditions for the macroscopic potential ψ are

$$\psi = \psi_1, \quad z = 0, \quad (10)$$

$$\psi = \psi_1 - \delta \psi, \quad z = L, \quad (11)$$

in reservoirs 1 and 2, respectively. The chemical potentials $\mu_{(\pm)}$ obey similar macroscopic boundary conditions between the upstream and the downstream reservoirs. Then, the Stokes equation can be written as

$$\nabla p^* + \bar{q}_v \nabla \psi + \bar{c}_{(+)} \nabla \mu_{(+)} + \bar{c}_{(-)} \nabla \mu_{(-)} = \eta \nabla^2 \mathbf{v}, \quad (12)$$

or, equivalently, in terms of electrochemical potential $\tilde{\mu}_{(\pm)} = \mu_{(\pm)}^0 + \mu_{(\pm)} \pm e\psi$ [Newman, 1991],

$$\nabla p^* + \bar{c}_{(+)} \nabla \tilde{\mu}_{(+)} + \bar{c}_{(-)} \nabla \tilde{\mu}_{(-)} = \eta \nabla^2 \mathbf{v}. \quad (13)$$

We can integrate the Stokes equation for the pore fluid in cylindrical coordinates. The standard potentials $\mu_{(\pm)}^0$ depend on the choice of the standard values for the concentrations, electrostatic potential, and fluid pressure. We first see from equation (12) that there are three forcing terms in the Stokes equation: (1) the effective fluid pressure gradient, (2) the electrical field associated with external sources $\bar{q}_v \nabla \psi$, and (3) the chemical potential gradients associated with the ionic species. Therefore, the velocity can be divided into three components, including the mechanical, the electrical, and the chemiosmotic contributions,

$$\mathbf{v} = \mathbf{v}_m + \mathbf{v}_e + \mathbf{v}_c. \quad (14)$$

The boundary condition for the mechanical contribution is $\mathbf{v}_m(r=R) = 0$ on the surface of the capillary. We use identical boundary conditions for the other two velocity fields. This implies that the migration of the counterions in the Stern layer does not significantly influence this boundary condition, an assumption that may not be valid if the velocity of the pore water is too small. In addition, we will show that the contribution of the Stern layer can be neglected for DC conditions (because of the discontinuity of the solid phase); therefore, the boundary conditions for the velocity used above is correct.

[13] In the capillary model shown in Figure 1, the effective fluid pressure, the electromotive potential ψ , and the chemical potentials $\mu_{(\pm)}$ depend only on the distance z along the capillary,

$$p^*(z) = -\frac{\delta p^*}{L} z + p^*_1, \quad (15)$$

$$\psi(z) = -\frac{\delta \psi}{L} z + \psi_1, \quad (16)$$

$$\mu_{(\pm)}(z) = -\frac{\delta \mu_{(\pm)}}{L} z + \mu_{(\pm)}^1. \quad (17)$$

The average concentrations in the pore space of the capillary can be determined from the TMS model using the equality between the electrochemical potentials in the pore space and with a fictitious reservoir of ions in local equilibrium with the pore space of the capillary (see Appendix A). The excess of charge and the concentrations in the capillary are related by

$$\bar{q}_v = e(\bar{c}_{(+)} - \bar{c}_{(-)}), \quad (18)$$

$$\bar{c}_{(\pm)} = C_f \left(\sqrt{\frac{\bar{q}_v^2}{4C_f^2 e^2} + 1} \pm \frac{\bar{q}_v}{2eC_f} \right), \quad (19)$$

$$\bar{c}_{(\pm)} = C_f \left(\sqrt{\frac{Q_s^2}{e^2 R^2 C_f^2} + 1} \mp \frac{Q_s}{eRC_f} \right), \quad (20)$$

where equation (2) has been used and e is the elementary charge (1.6×10^{-19} C). The three contributions to the velocity of the pore water are

$$v_m(r) = -\left(\frac{r^2 - R^2}{4\eta} \right) \frac{\delta p^*}{L}, \quad (21)$$

$$v_e(r) = -\left(\frac{r^2 - R^2}{4\eta} \right) \bar{q}_v \frac{\delta \psi}{L}, \quad (22)$$

$$v_c(r) = -\left(\frac{r^2 - R^2}{4\eta} \right) \left(\bar{c}_{(+)} \frac{\delta \mu_{(+)}}{L} + \bar{c}_{(-)} \frac{\delta \mu_{(-)}}{L} \right). \quad (23)$$

The total velocity can be integrated to get the flux of the pore water through the capillary,

$$u = \int_0^R v(r) 2\pi r dr, \quad (24)$$

$$u = -\left(\frac{\pi R^4}{8\eta} \right) \left(\frac{\delta p^*}{L} + \bar{q}_v \frac{\delta \psi}{L} + \bar{c}_{(+)} \frac{\delta \mu_{(+)}}{L} + \bar{c}_{(-)} \frac{\delta \mu_{(-)}}{L} \right). \quad (25)$$

If we have a set of n capillaries of the same radius R over a cross section of surface area A , the porosity is defined as

$$\phi = \frac{n\pi R^2}{A}. \quad (26)$$

This equation is valid for n parallel capillaries; otherwise the parameter R is an apparent radius. The macroscopic flux density over the cross section of surface area A is therefore given by

$$U = \frac{nu}{A}, \quad (27)$$

$$U = -\frac{n}{A} \left(\frac{\pi R^4}{8\eta} \right) \left(\frac{\delta p^*}{L} + \bar{q}_v \frac{\delta \psi}{L} + \bar{c}_{(+)} \frac{\delta \mu_{(+)}}{L} + \bar{c}_{(-)} \frac{\delta \mu_{(-)}}{L} \right), \quad (28)$$

$$U = -\phi \left(\frac{R^2}{8\eta} \right) \left(\frac{\delta p^*}{L} + \bar{q}_v \frac{\delta \psi}{L} + \bar{c}_{(+)} \frac{\delta \mu_{(+)}}{L} + \bar{c}_{(-)} \frac{\delta \mu_{(-)}}{L} \right). \quad (29)$$

If we consider the effect of the tortuosity of the capillaries, we need to replace the porosity by an effective porosity, which is the ratio of the porosity to the tortuosity of the pore space α [Revil and Cathles, 1999; Jackson, 2008, 2010; Mohajeri et al., 2010]. This ratio is equivalent to the inverse of the formation factor F used to describe the in-phase conductivity of the porous material [Pride, 1994; Revil and Cathles, 1999],

$$F = \frac{\alpha}{\phi}. \quad (30)$$

In porous media, F is usually correlated to the connected porosity via a power law relationship named Archie's law,

$$F = \phi^{-m}, \quad (31)$$

where m is loosely called the cementation exponent [Archie, 1942].

[14] Darcy's law is defined as a linear relationship between the volumetric flux of water and the pressure gradient,

$$\mathbf{U} = -\left(\frac{k}{\eta}\right)\nabla p, \quad (32)$$

when the other potential gradients are equal to zero ($\delta\psi = \delta\mu_{(\pm)} = 0$) and in the absence of ions in the pore water. A comparison between equations (30) and (32) reveals a well-known expression of the permeability for a set of capillaries of radius R [e.g., *Ishido and Mizutani*, 1981; *Dullien*, 1992; *Jackson*, 2008, 2010],

$$k = \frac{\phi}{\alpha} \left(\frac{R^2}{8}\right) = \frac{R^2}{8F}, \quad (33)$$

and R is often called the hydraulic radius when equation (33) is applied to a real porous material. Therefore, the macroscopic constitutive equations for the Darcy velocity is

$$\mathbf{U} = -\left(\frac{k}{\eta}\right)(\nabla p^* - \bar{q}_V \mathbf{E} + \bar{c}_{(+)} \nabla \mu_{(+)} + \bar{c}_{(-)} \nabla \mu_{(-)}) \quad (34)$$

or, alternatively,

$$\mathbf{U} = -\left(\frac{k}{\eta}\right)(\nabla p^* + \bar{c}_{(+)} \nabla \tilde{\mu}_{(+)} + \bar{c}_{(-)} \nabla \tilde{\mu}_{(-)}), \quad (35)$$

where $\mathbf{E} = -\nabla \psi$ is the macroscopic electrical field and $\tilde{\mu}_{(\pm)} = \mu_{(\pm)}^0 + k_b T \ln C_{(\pm)} \pm e\psi$ are the macroscopic electrochemical potentials of the two charge carriers. If we use the equality of the macroscopic chemical potential gradients through the porous material, we obtain

$$\nabla \mu_{(+)} = \nabla \mu_{(-)} = \nabla \mu_f = k_b T \nabla \ln C_f. \quad (36)$$

Equation (36) is only valid for a 1:1 electrolyte. Combining equations (35) and (36), we can write the macroscopic equation for the Darcy velocity as

$$\mathbf{U} = -\left(\frac{k}{\eta}\right)[\nabla p^* - \bar{q}_V \mathbf{E} + (\bar{c}_{(+)} + \bar{c}_{(-)}) \nabla \mu_f]. \quad (37)$$

We now turn our attention to the flux densities of the cations and anions. These flux densities are related to diffusion, electromigration, and advective transport of the ionic species. The Nernst-Planck equation is written locally as (see Appendix A)

$$\mathbf{j}_{(\pm)} = -b_{(\pm)} \bar{c}_{(\pm)} \nabla \tilde{\mu}_{(\pm)} + \bar{c}_{(\pm)} \mathbf{v}_m, \quad (38)$$

$$\mathbf{j}_{(\pm)} = -b_{(\pm)} \bar{c}_{(\pm)} \nabla [(\pm e)\psi + k_b T C_{(\pm)}] + \bar{c}_{(\pm)} \mathbf{v}_m, \quad (39)$$

where $b_{(\pm)}$ represents the mobility of the ionic species in the pore water. Equation (38) is correct in the pore water (including the effect of the diffuse layer), but it does not take into account transport along the mineral surface (in the so-called Stern layer) by diffusion or by electromigration. The last term of equations (38) and (39) is related to the mechanical velocity. Indeed, the electrical and endosmotic velocities are already captured by the gradient of the electrochemical potential of the ionic species in the first term on the right-hand side of equations (38) and (39). In reference to the Stern layer contribution, the diffusion and the electromigration

components should comprise two terms: one contribution from the bulk of the capillary and one contribution along the mineral surface in the Stern layer [*Revil and Leroy*, 2004]. The Stern layer contribution has been suggested by *Zukoski and Saville* [1986a, 1986b] and is modeled in Appendix B. We add this contribution for completeness, but we will show in section 3 that it is not required to explain the transport properties of a clay rock, for which the solid phase is discontinuous. However, adding the Stern layer contribution would be helpful in order to model induced polarization, that is, the frequency dependence of electrical conductivity [*Revil and Florsch*, 2010; *Vaudelet et al.*, 2011].

[15] Using these two contributions, the flux densities of cations and anions are given by

$$\mathbf{j}_{(\pm)} = -b_{(\pm)} \bar{c}_{(\pm)} \nabla \tilde{\mu}_{(\pm)} - b_{(\pm)}^S \Gamma_{(\pm)} \nabla \tilde{\mu}_{(\pm)}^S \delta(r-R) + \bar{c}_{(\pm)} \mathbf{v}_m, \quad (40)$$

$$\mathbf{j}_{(\pm)} = -k_b T \left[b_{(\pm)} \bar{c}_{(\pm)} \nabla \ln C_{(\pm)} + b_{(\pm)}^S \Gamma_{(\pm)} \nabla \ln \Gamma_{(\pm)} \delta(r-R) \right] - (\pm e) \left[b_{(\pm)} \bar{c}_{(\pm)} + b_{(\pm)}^S \Gamma_{(\pm)} \delta(r-R) \right] \nabla \psi + \bar{c}_{(\pm)} \mathbf{v}_m, \quad (41)$$

where $b_{(\pm)}^S$ represents the mobilities of the ionic species along the mineral surface, $\Gamma_{(\pm)}$ are the surface concentration densities of cations and anions adsorbed on the mineral surface, $\tilde{\mu}_{(\pm)}^S$ represents the electrochemical potential along the mineral surface, and $\delta(r-R) = 0$ if $r \neq R$ and $\delta(r-R) = 1$ if $r = R$ ($0 \leq r \leq R$). In Appendix B, we demonstrate that

$$\nabla \tilde{\mu}_{(\pm)}^S = \nabla \tilde{\mu}_{(\pm)}; \quad (42)$$

that is, the gradient of the electrochemical potential along the mineral surface is equal to the gradient of the electrochemical potential in the pore water. This result is valid only if the solid phase is continuous at the scale of the representative elementary volume. The macroscopic ionic fluxes are defined by averaging the previous expression over a set of capillaries of the same radius R . After straightforward algebraic manipulations, this yields

$$\mathbf{J}_{(\pm)} = \frac{n\pi R^2}{A} \left\{ -b_{(\pm)} \bar{c}_{(\pm)} \nabla \tilde{\mu}_{(\pm)} + \bar{c}_{(\pm)} \mathbf{v}_m \right\} + \frac{n2\pi R}{A} \left[-b_{(\pm)}^S \Gamma_{(\pm)} \nabla \tilde{\mu}_{(\pm)} \right], \quad (43)$$

$$J_{(\pm)} = -\frac{n\pi R^2}{A} \left[k_b T \left(b_{(\pm)} \bar{c}_{(\pm)} + \frac{2}{R} b_{(\pm)}^S \Gamma_{(\pm)} \right) \frac{\delta \ln C_{(\pm)}}{L} + (\pm e) \left(b_{(\pm)} \bar{c}_{(\pm)} + \frac{2}{R} b_{(\pm)}^S \Gamma_{(\pm)} \right) \frac{\delta \psi}{L} \right] + \bar{c}_{(\pm)} U_m, \quad (44)$$

where U_m is the mechanical contribution to the Darcy velocity $\mathbf{U}_m = -(k/\eta)\nabla p^*$ and $\mathbf{J}_{(\pm)} = J_{(\pm)} \mathbf{z}$. Using the expression for the porosity, scaling the porosity by the tortuosity, and replacing the ratio of the porosity to the tortuosity by the formation factor (see equation (30)), we obtain

$$J_{(\pm)} = -\frac{k_b T}{e^2} \sigma_{(\pm)} \frac{\delta \ln C_{(\pm)}}{L} - \frac{(\pm 1)}{e^2} \sigma_{(\pm)} \frac{\delta \psi}{L} + \bar{c}_{(\pm)} U_m, \quad (45)$$

$$\sigma_{(\pm)} = \frac{1}{F} \left(e\beta_{(\pm)} \bar{c}_{(\pm)} + \frac{2}{R} e\beta_{(\pm)}^S \Gamma_{(\pm)} \right), \quad (46)$$

where we have used an alternative definition of the ionic mobility, $\beta_{(\pm)} = b_{(\pm)}e$. In vectorial form, the macroscopic ionic flux densities are given by

$$\mathbf{J}_{(\pm)} = -\frac{1}{e^2}\sigma_{(\pm)}\nabla\tilde{\mu}_{(\pm)} + \bar{c}_{(\pm)}\mathbf{U}_m. \quad (47)$$

The electrical current density is defined as the total amount of charges passing through the porous material per unit time and per unit surface area. The diffusion flux is defined as the mean flux of cations and anions passing through the porous material per unit surface area and per unit time. These two quantities are therefore related to the ionic flux densities by

$$J = e(J_{(+)} - J_{(-)}), \quad (48)$$

$$J_d = \frac{1}{2}(J_{(+)} + J_{(-)}), \quad (49)$$

where $\mathbf{J} = J\mathbf{z}$ and $\mathbf{J}_d = J_d\mathbf{z}$. Using the expression of the mechanical contribution to Darcy's velocity, we obtain, in vectorial form, the following macroscopic constitutive equations:

$$\mathbf{J} = -\frac{1}{e}(\sigma_{(+)} - \sigma_{(-)})\nabla\mu_f + \sigma\mathbf{E} - \frac{k}{\eta}\bar{q}_v\nabla p^*, \quad (50)$$

$$\mathbf{J}_d = -\frac{\sigma}{2e^2}\nabla\mu_f + \frac{1}{2e}(\sigma_{(+)} - \sigma_{(-)})\mathbf{E} - \frac{1}{2}(\bar{c}_{(+)} + \bar{c}_{(-)})\frac{k}{\eta}\nabla p^*. \quad (51)$$

The material properties entering these equations are defined below. The electrical conductivity is given as

$$\sigma = \sigma_{(+)} + \sigma_{(-)}. \quad (52)$$

The conductivity can also be written as the sum of pore water and surface conductivity acting in parallel,

$$\sigma = \frac{1}{F}(\bar{\sigma}_f + \sigma_S), \quad (53)$$

where the effective pore water conductivity and the surface conductivity are given by

$$\bar{\sigma}_f = e(\beta_{(+)}\bar{c}_{(+)} + \beta_{(-)}\bar{c}_{(-)}), \quad (54)$$

$$\sigma_S = \frac{2}{R}e(\beta_{(+)}^S\Gamma_{(+)} + \beta_{(-)}^S\Gamma_{(-)}), \quad (55)$$

where $\beta_{(\pm)} = b_{(\pm)}e$. The conductivity can be written as

$$\sigma = \frac{1}{F}\left(\bar{\sigma}_f + \frac{2}{R}\Sigma_S\right), \quad (56)$$

where Σ_S is the specific surface conductivity of the Stern layer (in S), defined by *Revil and Leroy* [2004] as

$$\Sigma_S = e(\beta_{(+)}^S\Gamma_{(+)} + \beta_{(-)}^S\Gamma_{(-)}). \quad (57)$$

Equation (56) may look like the equation derived by *Pfannkuch* [1972], but *Pfannkuch* [1972] did not separate the contribution of the diffuse and Stern layers. Therefore,

equation (56) bears quite a different meaning with respect to the equations developed by *Pfannkuch* [1972] and *Jackson* [2008, 2010]. Section 2.2 generalizes the previous equations to the case of a pore size distribution.

2.2. Generalization to a Pore Size Distribution

[16] We define $g(R)$ as the probability density to have a capillary with a radius between R and $R + dR$. Because $g(R)$ is normalized, we have

$$\int_0^\infty g(R)dR = 1. \quad (58)$$

We write the different raw moments of this probability distribution as

$$\Pi_n = \int_0^\infty R^n g(R)dR, \quad (59)$$

where n is a negative or positive integer (Π_n is the expectation of the distribution R^n according to the probability distribution $g(R)$). From equation (59), we have

$$\Pi_0 = \int_0^\infty g(R)dR = 1, \quad (60)$$

$$\Pi_1 = \int_0^\infty R g(R)dR, \quad (61)$$

$$\Pi_2 = \int_0^\infty R^2 g(R)dR, \quad (62)$$

and so on. When $g(R)$ is a delta distribution, we recover the case investigated in section 2.1.

[17] To proceed with our model, we first need to come back to the description of the concentration of the cations and anions as a function of the radius of the pore. With the Donnan approximation, the average concentrations of cations and anions in the pore space of a single capillary of radius R are (Appendix A)

$$\bar{c}_{(\pm)} = C_f\left(\sqrt{1 + \xi^2} \pm \xi\right), \quad (63)$$

$$\xi = \frac{Q_S}{eRC_f}. \quad (64)$$

For a distribution of pore radii described by $g(R)$, the (average) porosity, the macroscopic volumetric charge density \bar{Q}_V (in C m⁻³), and the macroscopic concentrations $\bar{C}_{(\pm)}$ (C m⁻³) are related to the raw moments of the pore size distribution by (Appendix C)

$$\phi = \frac{n\pi}{A}\Pi_2, \quad (65)$$

$$\bar{Q}_V = -2Q_S\frac{\Pi_1}{\Pi_2}, \quad (66)$$

$$\bar{C}_{(\pm)} = C_f\left(\sqrt{1 + \Theta^2} \pm \Theta\right), \quad (67)$$

respectively, where the dimensionless parameter Θ is defined by

$$\Theta \equiv \frac{Q_s \Pi_1}{e C_f \Pi_2}. \quad (68)$$

This coefficient will be the main dimensionless coefficient controlling the dependence on salinity of some of the material properties entering the constitutive equations. The osmotic pressure is given by equation (11), with \bar{Q}_V replacing \bar{q}_V . The parameters \bar{Q}_V , $\bar{C}_{(\pm)}$, and Θ are the macroscopic equivalents of the capillary-scale properties \bar{q}_V , $\bar{c}_{(\pm)}$, and ξ , respectively.

[18] As in section 2.1, the flux density (Darcy velocity) over a cross section of the porous material of surface area A is written as

$$U = \frac{nu}{A}, \quad (69)$$

$$u = -\left(\frac{\pi \Pi_4}{8\eta}\right) \left(\frac{\delta p^*}{L} + \bar{Q}_V \frac{\delta \psi}{L} + \bar{C}_{(+)} \frac{\delta \mu_{(+)}}{L} + \bar{C}_{(-)} \frac{\delta \mu_{(-)}}{L} \right). \quad (70)$$

Carrying out the convolution product, adding the tortuosity effect (and therefore introducing the formation factor), using the definitions above, the Darcy velocity is given by

$$U = -\frac{k}{\eta} \left[\frac{\delta p^*}{L} + \bar{Q}_V \frac{\delta \psi}{L} + \bar{C}_{(+)} \frac{\delta \mu_{(+)}}{L} + \bar{C}_{(-)} \frac{\delta \mu_{(-)}}{L} \right], \quad (71)$$

where the (hydrodynamic) permeability is related to two raw moments of the pore size distribution by

$$k = \frac{1}{8F} \frac{\Pi_4}{\Pi_2}. \quad (72)$$

Equation (72) is actually well known and has been derived by several authors [see, e.g., *Dullien*, 1992; *Jackson*, 2008, and references therein]. In vectorial notation, equation (71) is written as

$$\mathbf{U} = -\frac{k}{\eta} [\nabla p^* + \bar{Q}_V \nabla \psi + \bar{C}_{(+)} \nabla \mu_{(+)} + \bar{C}_{(-)} \nabla \mu_{(-)}]. \quad (73)$$

The Darcy velocity comprises the hydromechanical contribution, including an osmotic pressure term (the first term in the brackets), the electroosmotic contribution (the second term), and the chemiosmotic contributions (the last two terms). The relationship between the macroscopic excess of electrical charges (from the diffuse layer) in the pore space and the concentrations of cations and anions in the pore space of the material is

$$\bar{Q}_V = e(\bar{C}_{(+)} - \bar{C}_{(-)}). \quad (74)$$

Combining equations (74) and (73), the constitutive equation for the Darcy velocity is given by

$$\mathbf{U} = -\frac{k}{\eta} [\nabla p^* + \bar{C}_{(+)} \nabla \tilde{\mu}_{(+)} + \bar{C}_{(-)} \nabla \tilde{\mu}_{(-)}]. \quad (75)$$

Applying the same rules to the ionic densities, we obtain the same macroscopic equation as in the case of capillaries of

the same pore radius. We can write the final macroscopic constitutive equations in a matrix form:

$$\begin{bmatrix} 2\mathbf{J}_d \\ \mathbf{J} \\ \mathbf{U} \end{bmatrix} = -\bar{\mathbf{M}} \begin{bmatrix} \nabla \mu_f \\ \nabla \psi \\ \nabla p^* \end{bmatrix}, \quad (76)$$

$$\bar{\mathbf{M}} = \begin{bmatrix} \frac{\sigma}{e^2} & \frac{1}{e}(\sigma_{(+)} - \sigma_{(-)}) & \frac{k}{\eta}(\bar{C}_{(+)} + \bar{C}_{(-)}) \\ \frac{1}{e}(\sigma_{(+)} - \sigma_{(-)}) & \sigma & \frac{k}{\eta}\bar{Q}_V \\ \frac{k}{\eta}(\bar{C}_{(+)} + \bar{C}_{(-)}) & \frac{k}{\eta}\bar{Q}_V & \frac{k}{\eta} \end{bmatrix}, \quad (77)$$

where $\bar{\mathbf{M}}$ is a matrix of material properties (note that for an anisotropic material, each element of $\bar{\mathbf{M}}$ would be a second-order symmetric tensor). The matrix $\bar{\mathbf{M}}$ obeys Onsager reciprocity $M_{ij} = M_{ji}$ [*Prigogine*, 1947].

[19] The material properties entering the matrix $\bar{\mathbf{M}}$ are defined by equations (80)–(85). The concentrations $\bar{C}_{(\pm)}$ are given by the TMS model (see Appendix A). The electrical conductivity and the contributions to the total electrical conductivity are defined by

$$\sigma = \sigma_{(+)} + \sigma_{(-)}, \quad (78)$$

$$\sigma_{(\pm)} = \frac{1}{F} \left(e\beta_{(\pm)}\bar{C}_{(\pm)} + 2\frac{\Pi_1}{\Pi_2} e\beta_{(\pm)}^S \Gamma_{(\pm)} \right), \quad (79)$$

respectively. The conductivity can, therefore, be written as the sum of pore water and surface conductivity acting in parallel, as proposed by *Waxman and Smits* [1968],

$$\sigma = \frac{1}{F} (\bar{\sigma}_f + \sigma_s), \quad (80)$$

where the effective pore water conductivity and the surface conductivity are given by

$$\bar{\sigma}_f = e(\beta_{(+)}\bar{C}_{(+)} + \beta_{(-)}\bar{C}_{(-)}), \quad (81)$$

$$\sigma_s = 2\frac{\Pi_1}{\Pi_2} e(\beta_{(+)}^S \Gamma_{(+)} + \beta_{(-)}^S \Gamma_{(-)}). \quad (82)$$

Equation (80) is a Waxman and Smits type equation, except that the conductivity of the pore water is distinct from the conductivity of a reservoir in local equilibrium with the porous material. *Bussian* [1983] and *Revil et al.* [1998] have shown that this equation works well as long as the connectivity problem is ignored. Indeed, in a complex porous material, the surface and bulk tortuosities are different [see also *Schwartz et al.*, 1989; *Bernabé and Revil*, 1995; *Bernabé*, 1998]. For a bundle of capillaries, the electrical conductivity can be written as (Appendix C)

$$\sigma = \frac{1}{F} \left(\bar{\sigma}_f + 2\frac{\Pi_1}{\Pi_2} \Sigma_S \right). \quad (83)$$

This equation is distinct from the equation derived by previous authors [see, e.g., *Pride*, 1994] because the conductivity of the diffuse layer is encapsulated in the effective pore water conductivity and the surface conductance is only due to the contribution of the Stern layer. The relation between electrical conductivity and permeability is discussed in Appendix D.

[20] In the past, a number of researchers [e.g., *Pride*, 1994] have looked for a relationship between the electrical conductivity and the permeability of porous rocks. In Appendix D, we test a widely used relationship between the permeability and two parameters derived from the electrical conductivity equation, and we explain why this classical formula is expected to fail for porous material characterized by broad or multimodal pore size distributions.

2.3. Introduction of Hydrodynamic Dispersion

[21] We should keep in mind that there are limitations in the use of the bundle of nonconnecting capillary tubes model. The assumptions made in this model are the following: (1) the connectivity of the pores is ignored, (2) the solid phase is assumed continuous through the two reservoirs, i.e., at the scale of a representative elementary volume, and (3) the thickness of the diffuse layer is on the same order of magnitude as the size of the pores.

[22] The previous transport model does not account for hydrodynamic dispersion. In fact, because the pores do not intersect in the capillary model, the model cannot explain transversal dispersivity. However, if we consider the migration of a salt plume in a porous material, we have to include the dispersion effect associated with mixing. We use below a classical Fickian approach where the diffusion coefficient appearing in the first Fick's law is replaced by an effective dispersion tensor accounting for both diffusion and hydrodynamic longitudinal and transversal dispersion coefficients. From equation (76), the electrical field can be written as a function of the current density \mathbf{J} and the Darcy velocity \mathbf{U} as

$$\mathbf{E} = \frac{1}{\sigma} \mathbf{J} + \frac{1}{e} (T_{(+)} - T_{(-)}) \nabla \mu_f + \frac{\bar{Q}_V k}{\sigma \eta} \nabla p^*, \quad (84)$$

where the macroscopic Hittorf numbers are defined by

$$T_{(\pm)} = \frac{\sigma_{(\pm)}}{\sigma}. \quad (85)$$

Taking the expression of the flux of salt and after algebraic manipulations, we obtain

$$\mathbf{J}_d = -D \nabla C_f + \frac{1}{2e} (2T_{(+)} - 1) \left(\mathbf{J} + \frac{\bar{Q}_V k}{\eta} \nabla p^* \right) - \frac{k}{2\eta} (\bar{C}_{(+)} + \bar{C}_{(-)}) \nabla p^*, \quad (86)$$

$$D = \frac{2k_b T}{e^2 C_f} \frac{\sigma_{(+)} \sigma_{(-)}}{\sigma_{(+)} + \sigma_{(-)}}. \quad (87)$$

In this equation, D is the diffusion coefficient of the salt through the porous material. This approach was first derived by *Revil et al.* [1996] and *Revil* [1999], and it generalizes the Nernst-Hartley equation of brines used to compute the mutual diffusion coefficient of a binary salt in an electrolyte. Now we

can replace D in equation (86) by the Fickian hydrodynamic dispersion tensor $\bar{\mathbf{D}}$, defined as

$$\bar{\mathbf{D}} = [D + \alpha_T U] \mathbf{I}_3 + \frac{\alpha_L - \alpha_T}{U} \mathbf{U} \otimes \mathbf{U}, \quad (88)$$

$$U = |\mathbf{U}|, \quad (89)$$

where $\mathbf{a} \otimes \mathbf{b}$ represents the tensorial product between vectors \mathbf{a} and \mathbf{b} , and α_L and α_T are the longitudinal (along \mathbf{U}) and transverse (normal to \mathbf{U}) dispersivities (in m). The final constitutive equations for the salt flux density, the Darcy velocity, and the current density are therefore

$$\mathbf{J}_d = -\bar{\mathbf{D}} \cdot \nabla C_f + \frac{1}{2e} (2T_{(+)} - 1) \left(\mathbf{J} + \frac{\bar{Q}_V k}{\eta} \nabla p^* \right) - \frac{k}{2\eta} (\bar{C}_{(+)} + \bar{C}_{(-)}) \nabla p^*, \quad (90)$$

$$\mathbf{U} = - \left(\frac{k}{\eta} \right) [\nabla p^* - \bar{Q}_V \mathbf{E} + (\bar{C}_{(+)} + \bar{C}_{(-)}) \nabla \mu_f], \quad (91)$$

$$\mathbf{J} = - \frac{1}{e} (\sigma_{(+)} - \sigma_{(-)}) \nabla \mu_f + \sigma \mathbf{E} - \frac{\bar{Q}_V k}{\eta} \nabla p^*. \quad (92)$$

These equations are valid for any porous material.

3. Application to Transport Properties of Clay Materials

[23] One application of the present theory is to predict the coupled flow in clay media. We chose the Callovo-Oxfordian (COx) clay rock to test our model because it is well-characterized clay material. This clay rock is under consideration for the long-term storage of nuclear wastes in the Paris Basin (France) [*Yven et al.*, 2006], and its properties have been investigated by several researchers [e.g., *Sammartino et al.*, 2003; *Delay and Distinguin*, 2004; *Jougnot et al.*, 2009, 2010a, 2010b; *Rousseau-Gueutin et al.*, 2010, and references therein]. The pore size distribution of this clay rock is shown in Figure 2. The Callovo-Oxfordian clay rock can be conceptualized as a clay matrix with some imbedded grains of silica and carbonates (calcite and a minor fraction of dolomite) (see Figure 3a). The clay matrix represents 20%–50% of the rock volume in the total formation (up to 45%–50% in the subunit C2b1). This clay fraction is mainly composed of illite and interstratified illite-smectite clays. There is also a small amount of kaolinite in the lower part of the formation. The size of the silica and carbonate grains is in the range of 10–20 μm . The volume of the silica and carbonate grains represents between 20% and 40% of the rock assemblage. In addition, there are small amounts of potassic feldspar, plagioclase, and pyrite. An extensive geochemical analysis of the Callovo-Oxfordian formation is given by *Gaucher et al.* [2004]. The properties of this clay rock are reported in Table 4, and the composition of the pore water is reported in Table 5.

[24] In sections 3.1 and 3.2, we first rework the theory in terms of measurable parameters. Then, we propose some comparisons between the theory and measured properties characterizing the COx clay rock, including the streaming potential coupling coefficient, the Hittorf number of the cations, the osmotic sensitivity coefficient, and the effective diffusion coefficient of the salt in a salinity gradient.

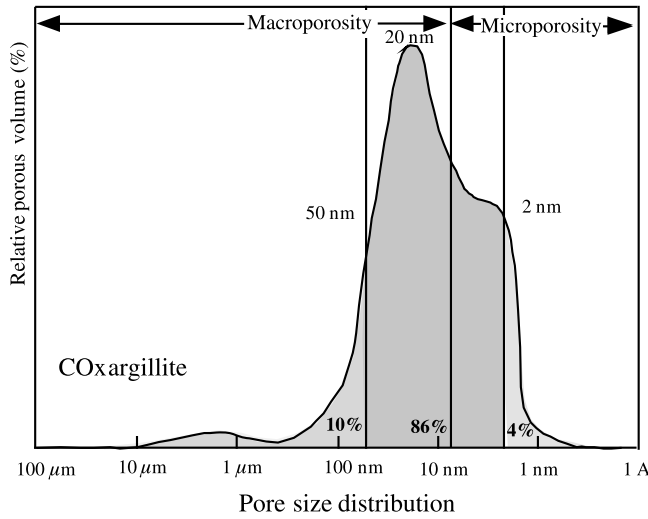


Figure 2. Pore size distribution of the Callovo-Oxfordian (COx) clay rock [Agence Nationale pour la Gestion des Déchets Radioactifs, 2005]. The peak of the distribution corresponds to a pore size of 20 nm. The distinction between the macroporosity and the microporosity is based on the thickness of the diffuse layer computed from the Debye length and the salinity of the ionic reservoir.

3.1. Measurable Transport Properties

[25] We are looking, first, for an expression for the so-called (nondimensional) osmotic efficiency ε . We will also explicitly write the formula for the streaming potential coupling coefficient and the macroscopic Hittorf number of the cations. We consider the case for which the total current density is zero (typically, the case of a cylindrical core sample between two reservoirs). Using $T_{(+)} + T_{(-)} = 1$ and equation (92), we obtain

$$\mathbf{E}|_{J=0} = \frac{1}{e} (2T_{(+)} - 1) \nabla \mu_f - \frac{\bar{Q}_V}{\sigma} \mathbf{U}_m, \quad (93)$$

where \mathbf{U}_m is the mechanical contribution to the Darcy velocity $\mathbf{U}_m = -(k/\eta) \nabla p^*$. The streaming potential coupling coefficient is defined as

$$C \equiv \left. \frac{\Delta \psi}{\Delta p} \right|_{J=0, \nabla \mu_f=0} = -\frac{\bar{Q}_V k}{\sigma \eta} = -\frac{\bar{Q}_V k F}{\eta \left(\bar{\sigma}_f + 2 \frac{\Pi_1}{\Pi_2} \Sigma_S \right)}. \quad (94)$$

Replacing the electrical field \mathbf{E} in equation (91) by the expression obtained in equation (93), we obtain the following expression for the Darcy velocity:

$$\mathbf{U} = -\left(\frac{k}{\eta}\right) \left\{ \nabla p^* - \bar{Q}_V \left[\frac{1}{e} (2T_{(+)} - 1) \nabla \mu_f - C \nabla p^* \right] + (\bar{C}_{(+)} + \bar{C}_{(-)}) \nabla \mu_f \right\}, \quad (95)$$

$$\mathbf{U} = -\left(\frac{k}{\eta}\right) \left\{ (1+a) \nabla (p - \pi) + \left[-\bar{Q}_V \frac{1}{e} (2T_{(+)} - 1) + (\bar{C}_{(+)} + \bar{C}_{(-)}) \right] \nabla \mu_f \right\}, \quad (96)$$

where the dimensionless coefficient a is defined as

$$a = C \bar{Q}_V. \quad (97)$$

Using the values of the parameters reported in Tables 4–7, we find that a is on the order of 2×10^{-2} and can, therefore, be neglected. We use now the Donnan model (see Appendix A) to obtain expressions for the concentrations in the pore space of the porous material:

$$\bar{C}_{(+)} + \bar{C}_{(-)} = 2C_f \sqrt{1 + \Theta^2}, \quad (98)$$

$$\Theta \equiv \frac{\bar{Q}_V}{2eC_f} = -\frac{Q_S}{eC_f} \frac{\Pi_1}{\Pi_2}. \quad (99)$$

In addition, the gradient of the chemical potential of the salt between the two reservoirs can be related to the gradients in salinity C_f and osmotic pressure between the two reservoirs by

$$\nabla \mu_f = k_b T \nabla \ln C_f = \left(\frac{1}{2C_f} \right) \nabla \pi. \quad (100)$$

Using equations (98) and (100) in equation (96) yields

$$\mathbf{U} = -\left(\frac{k}{\eta}\right) \left\{ \nabla p - \nabla \pi + \left[\Theta (1 - 2T_{(+)} + \sqrt{1 + \Theta^2}) \right] \nabla \pi \right\}. \quad (101)$$

We can write equation (101) in a more compact form as

$$\mathbf{U} = -\left(\frac{k}{\eta}\right) [\nabla p - \varepsilon \nabla \pi], \quad (102)$$

where the two material properties involved in equation (102) are related to the two dimensionless numbers $T_{(+)}$ and Θ by

$$\varepsilon = 1 - \Theta (1 - 2T_{(+)} - \sqrt{1 + \Theta^2}), \quad (103)$$

$$k^* = k / (1 + a), \quad (104)$$

where k^* is an apparent permeability corresponding to the intrinsic hydrodynamic permeability corrected for electro-osmosis [see Revil *et al.*, 2005]. For the COx clay rock, we have $k^* \approx k$ because $a \ll 1$. The coefficient ε is the (dimensionless) osmotic efficiency, defined by

$$\varepsilon \equiv \left(\frac{\partial p}{\partial \pi} \right)_{J, \mathbf{U}=0}. \quad (105)$$

Rousseau-Gueutin *et al.* [2010] also use the following expression for the Darcy velocity:

$$\mathbf{U} = -\frac{k^*}{\eta} \nabla p + \frac{k_c}{\eta} \nabla \pi, \quad (106)$$

where k_c is the osmotic permeability (in m^2). Comparing equations (102) and (106) yields $k_c = k^* \varepsilon \approx k \varepsilon$. Revil and Leroy [2004] demonstrated that the osmotic efficiency can also be estimated from ultrafiltration experiments [see also Malusis and Shackelford, 2004].

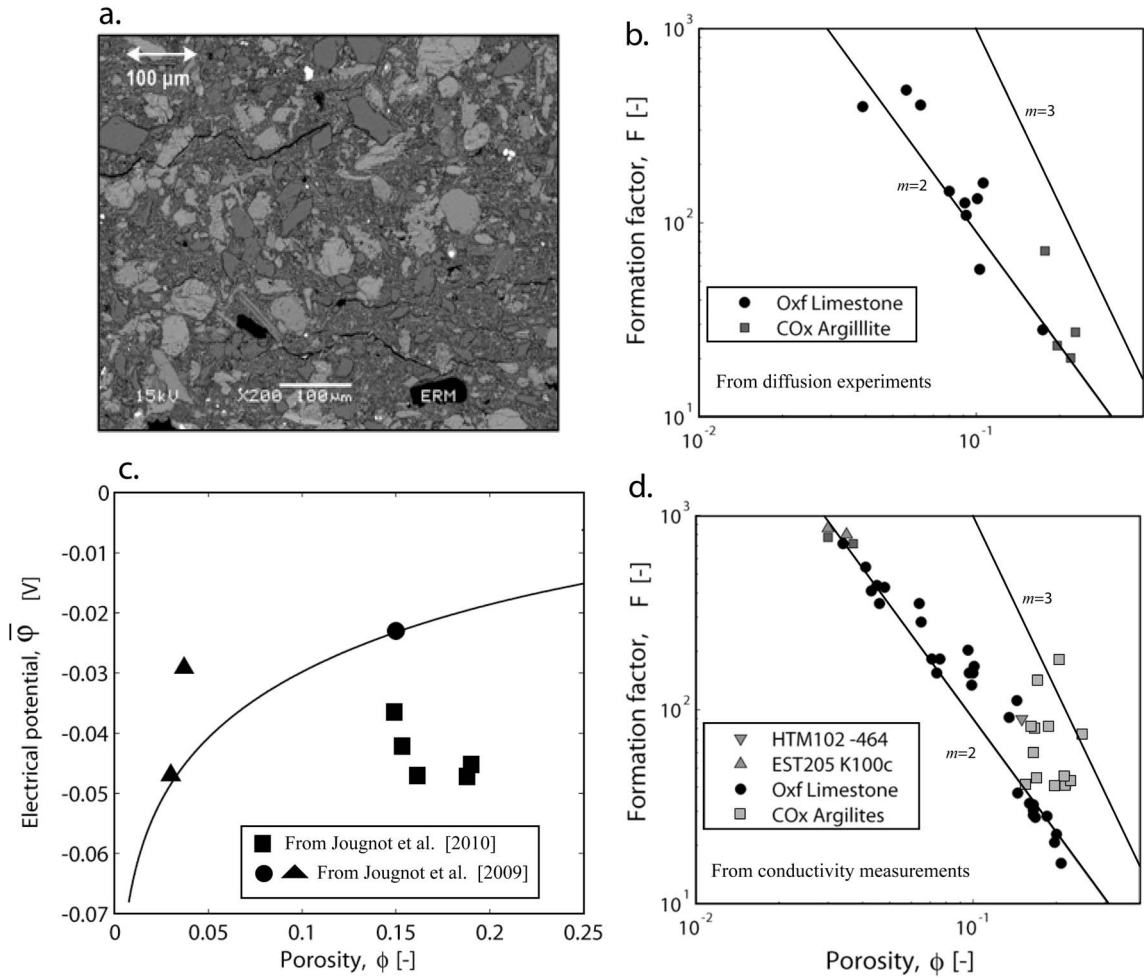


Figure 3. Mean potential and formation factor of the COx clay rock. (a) COx sample analyzed by scanning electron microscopy (photo from J. C. Robinet). (b) Formation factor versus porosity from electrical conductivity measurement [Revil *et al.*, 2005]. (c) The mean electrical potential models computed from the pore water chemistry used for the diffusion experiments of Melkior *et al.* [2007] (solid line). The experimental points are from Jougnot *et al.* [2010b, Tables 4 and 5]. (d) Formation factor obtained by the ratio $F = D_{\text{HTO}}^i / D_{\text{HTO}}$ (D_{HTO}^i is the diffusion coefficient of HTO in water, and D_{HTO} is the diffusion coefficient of hydrogen tritium oxygen (tritiated water) in the core samples). Data are from Descostes *et al.* [2008]; Oxf stands for Oxfordian.

3.2. Comparison Between Experimental Data and Theory

[26] We are now in a position to compare some material properties of the COx clay rock with our model. We first determine some of the raw moments of the pore size distribution for the COx argillite. Using equation (72) for the permeability and the mean value of the porosity and mean value cementation exponent reported in Table 4, we obtain $\Pi_4/\Pi_2 = 1 \times 10^{-17} \text{ m}^2$. If the pore size distribution is described by a delta function $\Pi_4/\Pi_2 = R^2$, this yields a mean pore size $R = 32 \pm 8 \text{ nm}$. This value is slightly above the peak of the pore size distribution (20 nm; see Figure 2).

[27] The mean volumetric charge density of the diffuse layer is given by $\bar{Q}_V = 8 \times 10^6 \text{ C m}^{-3}$ (see Revil *et al.* [2005, Table 5], who corrects these values by assuming that 90% of the countercharge is located in the Stern layer, as predicted by the triple-layer model of Leroy *et al.* [2007]). The surface charge density on the mineral surface Q_0 can be obtained from the ratio of the cation exchange capacity (CEC) and the

specific surface area reported in Table 4. This yields $Q_0 \approx 2$ elementary charge nm^{-2} (0.32 C m^{-2}), a value that agrees with the mean surface charge of clay minerals [Patchett, 1975; Revil *et al.*, 1998]. Typically, 90% of this surface

Table 4. Material Properties of the Callovo-Oxfordian (COx) Clay Rock

Symbol	Definition	Value	Source ^a
$\bar{\varphi}$	Mean pore electrical potential	$-40 \pm 10 \text{ mV}$	1
m	Cementation exponent	2.5 ± 0.5	1
ϕ	Connected porosity	0.15 ± 0.08	2
$\log k$	Log permeability	-20 ± 1	3, 4
CEC	Cation exchange capacity	$0.18 \pm 0.08 \text{ mol kg}^{-1}$	5
ρ_g	Grains mass density	$2700 \pm 50 \text{ kg m}^{-3}$	5
S_{sp}^b	Specific surface area	$5 \times 10^4 \text{ m}^2 \text{ kg}^{-1}$	6

^aSources are as follows: 1, Jougnot *et al.* [2009]; 2, Descostes *et al.* [2008]; 3, Distinguin and Lavanchy [2007]; 4, Rousseau-Gueutin *et al.* [2010]; 5, Leroy *et al.* [2007]; 6, Gaucher *et al.* [2004].

^bThe confidence interval is not known.

Table 5. Callovo-Oxfordian Water Compositions for a Reservoir Locally in Equilibrium With the COx Clay Rock and for the Pore Water^a

THERMOAR Model ^b		Simplified Composition ^c		Pore Water Composition ^d	
Species	C_i (mol L ⁻¹)	Species	C_i (mol L ⁻¹)	Species	\bar{C}_i (mol L ⁻¹)
Na	32×10^{-3}	Na ⁺	31.5×10^{-3}	Na ⁺	149×10^{-3}
K	7×10^{-3}	K ⁺	6.5×10^{-3}	K ⁺	31×10^{-3}
Ca	15×10^{-3}	Ca ²⁺	9.5×10^{-3}	Ca ²⁺	214×10^{-3}
Mg	14×10^{-3}	Mg ²⁺	8.1×10^{-3}	Mg ²⁺	182×10^{-3}
Cl	30×10^{-3}	Cl ⁻	30×10^{-3}	Cl ⁻	6×10^{-3}
S(+6)	34×10^{-3}	SO ₄ ²⁻	21×10^{-3}	SO ₄ ²⁻	1×10^{-3}
pH	7.3	—	—	pH	6.6
pCO ₂	-2.51	HCO ₃ ⁻	1.2×10^{-3}	HCO ₃ ⁻	1.2×10^{-3}

^aFor COx clay rock, see *Leroy et al.* [2007, Table 4]; for pore water, see this work.

^bSee *Gaucher et al.* [2006].

^cObtained using PHREEQC2 (see *Leroy et al.* [2007]). The PHREEQC2 software is described by *Parkhurst and Appelo* [1999]. Note that only charged species are used.

^dComputed using the Teorell-Sievers-Meyer model assuming a mean potential of -40 mV (see Table 4 and Figure 2b). Note that only charged species are used.

charge is compensated in the Stern layer (see the electrical double-layer modeling by *Leroy and Revil* [2009]). This yields $Q_S = -0.032 \text{ C m}^{-2}$.

[28] We now compare our model to measurements of the streaming potential coupling coefficient. The relationship between the conductivity of the pore water $\bar{\sigma}_f$ and the conductivity of the reservoir in contact with the charged porous material σ_f is given approximately by [*Revil and Leroy*, 2004]

$$\bar{\sigma}_f \approx \sigma_f \sqrt{1 + \Theta^2}. \quad (107)$$

Therefore, using equation (94), the coupling coefficient can be expressed as

$$C = - \frac{\bar{Q}_V kF}{\eta \left(\sigma_f \sqrt{1 + \Theta} + 2 \frac{\Pi_1}{\Pi_2} \Sigma_S \right)}. \quad (108)$$

If the experiments are performed at a time scale that is not compatible with the sorption or desorption of ionic species in the Stern layer, the Stern layer contribution should be neglected. The streaming potential experiments performed

Table 6. Conductivity of the Pore Water of the COx Clay Rock^a

Species	\bar{C}_i (mol L ⁻¹)	β_i^b ($10^{-8} \text{ m}^2 \text{ s}^{-1} \text{ V}^{-1}$)	$\bar{\sigma}_i$ (S m ⁻¹)
Na ⁺	149×10^{-3}	5.2	0.75
K ⁺	31×10^{-3}	7.6	0.23
Ca ²⁺	214×10^{-3}	3.1	1.28
Mg ²⁺	182×10^{-3}	2.7	0.95
Cl ⁻	6×10^{-3}	7.9	0.05
SO ₄ ²⁻	1×10^{-3}	4.4	0.01

^aThe pore conductivity is computed from the concentrations and mobilities of the ionic species present in the pore space. The average pore water conductivity is 3.3 S m^{-1} (at 25°C), which corresponds to the sum of all the ionic contributions.

^bValues are from *Robinson and Stokes* [1965] (at 25°C).

Table 7. Results of the Osmotic Efficiency Estimates Reported by *Rousseau-Gueutin et al.* [2010] From Chemical Pulse Tests and Comparison With the Present Model

Salinity, NaCl (molecules L ⁻¹)	Θ^a	Value of ε	
		Measured	Predicted
1.7	0.028	0.0010	0.0004
0.43	0.111	0.012	0.006
0.12	0.399	0.055	0.071
0.086	0.557	0.12	0.13
0.086	0.557	0.087	0.13
0.086	0.557	0.13	0.13

^aUsing $\text{CEC} = 0.10 \text{ molecules kg}^{-1}$ (0.10 meq g^{-1}), $f_Q = 0.90$, $\phi = 0.22$.

by *Revil et al.* [2005] are usually done over a few minutes, a time scale that is much shorter than the time required for the kinetics of sorption to be efficient. Therefore, these experiments need to be compared with equation (108) without accounting for the Stern layer contribution, which leads to

$$C \approx - \frac{\bar{Q}_V kF}{\eta \sigma_f \sqrt{1 + \Theta}}. \quad (109)$$

A comparison between equation (109) and the experimental data reported by *Revil et al.* [2005] is reported in Figure 4. There is a good agreement between the theory and these experimental data. When the dimensionless number Θ is very small (at high salinities), the coupling coefficient is given by

$$\lim_{\Theta \ll 1} C \approx - \frac{\bar{Q}_V kF}{\eta \sigma_f}. \quad (110)$$

In this high-salinity limit ($\Theta \ll 1$), the streaming potential coupling coefficient is also given by the Helmholtz-Smoluchowski equation $C \approx \varepsilon_f \zeta / \eta \sigma_f$, where ζ (in V) is the zeta potential at the interface between the Stern and diffuse layers and ε_f is the dielectric constant of the pore water. The Helmholtz-Smoluchowski equation indicates that the coupling coefficient is independent of the microstructure at high salinities, implying that the volumetric charge density of the diffuse layer \bar{Q}_V should scale as $1/kF$. *Jardani et al.* [2007] found that for a large collection of core samples, \bar{Q}_V scales as $1/k$ over 11 orders of magnitude. For such a broad range of scales, the scaling between \bar{Q}_V and $1/kF$ may be masked in these data and should be investigated further.

[29] When the dimensionless number Θ is very large (at low salinities), we obtain

$$C \approx - \frac{2kF}{\eta (\beta_{(+)} + \beta_{(-)})}; \quad (111)$$

therefore, the coupling coefficient reaches a limiting value that depends only on the product of the formation factor by the permeability, and that is independent of the salinity and the volumetric charge density. So both the volumetric charge density and the product (kF) are uniquely determined by the streaming potential versus salinity curve (Figure 4a).

[30] We now focus on the value of the macroscopic Hittorf number. Using equation (85) with equations (76)

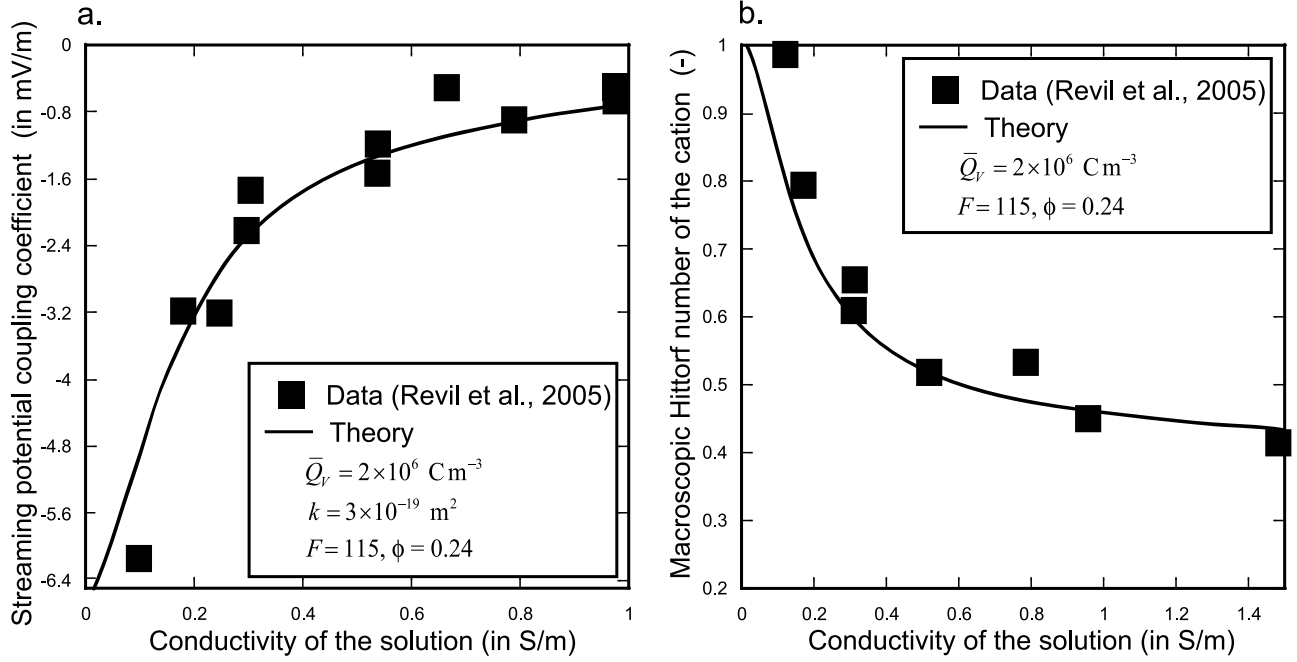


Figure 4. Streaming potential coupling coefficient (in mV m^{-1}) and macroscopic Hittorf number of the cation (dimensionless) versus the electrical conductivity of the solution used to perform the experiments. Only the high-porosity samples (samples 438, 480V, and 512) have been selected here with the same porosity range (mean of 0.24, SD of 0.02). (a) Streaming potential coupling coefficient. (b) Macroscopic Hittorf number of the cations. The theoretical curves do not account for Stern layer transport.

and (67), the Hittorf number of the cations can be related to the dimensionless number Θ as

$$T_{(+)} = \frac{\sigma_{(+)}}{\sigma_{(+)} + \sigma_{(-)}}, \quad (112)$$

$$T_{(+)} = \frac{\beta_{(+)}(\sqrt{1 + \Theta^2} + \Theta) + \beta_{(+)}^S \Psi}{\beta_{(+)}(\sqrt{1 + \Theta^2} + \Theta) + \beta_{(+)}^S \Psi + \beta_{(-)}(\sqrt{1 + \Theta^2} - \Theta)}, \quad (113)$$

where we have assumed that the Stern layer is mainly populated by positive ions (counterions) and $\Psi = 2\Pi_{-1}\Gamma_{(+)}C_f$ is a second dimensionless number related to the density of counterions in the Stern layer with respect to the salinity of the reservoir (the so-called Dukhin number). We need to estimate the Stern layer conductivity $2e\Pi_{-1}\beta_{(+)}^S\Gamma_{(+)}$. We already know that $e\Gamma_{(+)} = Q_\beta = |Q_0 - Q_S| = 0.29 \text{ C m}^{-2}$ (the surface charge density of the Stern layer). The value of the surface mobility in the Stern layer for the counterions must also be known. Taking $\beta_{(+)}^S = 5 \times 10^{-8} \text{ m}^2 \text{ V}^{-1} \text{ s}^{-1}$, we have, therefore, $2e(\Pi_{-1}/\Pi_2)\beta_{(+)}^S\Gamma_{(+)} \approx 4 \text{ S m}^{-1}$. With this value, the Hittorf numbers are strongly overpredicted (not shown). A comparison between the theory (without transport in the Stern layer) and the experimental data reported by *Revil et al.* [2005] is shown in Figure 4b (using the same samples used in Figure 4a). The line represents the prediction of the theory without the Stern layer. Therefore, it seems that the transport in the Stern layer does not play a role for the COX argillite and can be neglected. Consequently, the macro-

scopic Hittorf number of the cations can be determined by the following relationship:

$$T_{(+)} = \frac{\beta_{(+)}(\sqrt{1 + \Theta^2} + \Theta)}{\beta_{(+)}(\sqrt{1 + \Theta^2} + \Theta) + \beta_{(-)}(\sqrt{1 + \Theta^2} - \Theta)}. \quad (114)$$

In Figure 5, we plot the Hittorf number versus the dimensionless parameter Θ for the COx clay rock and for literature data for both shaly sands and porous glasses with known pore sizes. There is quite good agreement between the theory and the experimental data. In the case where the cations and the anions have roughly the same mobilities (e.g., KCl), the Hittorf number is given by the simplified equation

$$T_{(+)} \approx \frac{\sqrt{1 + \Theta^2} + \Theta}{2\sqrt{1 + \Theta^2}}. \quad (115)$$

We can now find an expression for the osmotic efficiency. Using equations (103) and (114), we find

$$\varepsilon = 1 + \Theta \left(\frac{\beta_{(+)}(\sqrt{1 + \Theta^2} + \Theta) - \beta_{(-)}(\sqrt{1 + \Theta^2} - \Theta)}{\beta_{(+)}(\sqrt{1 + \Theta^2} + \Theta) + \beta_{(-)}(\sqrt{1 + \Theta^2} - \Theta)} \right) - \sqrt{1 + \Theta^2}. \quad (116)$$

If the mobilities of the cations and anions are roughly the same, the osmotic efficiency is given by the simplified formula

$$\varepsilon = \frac{\sqrt{1 + \Theta^2} - 1}{\sqrt{1 + \Theta^2}}. \quad (117)$$

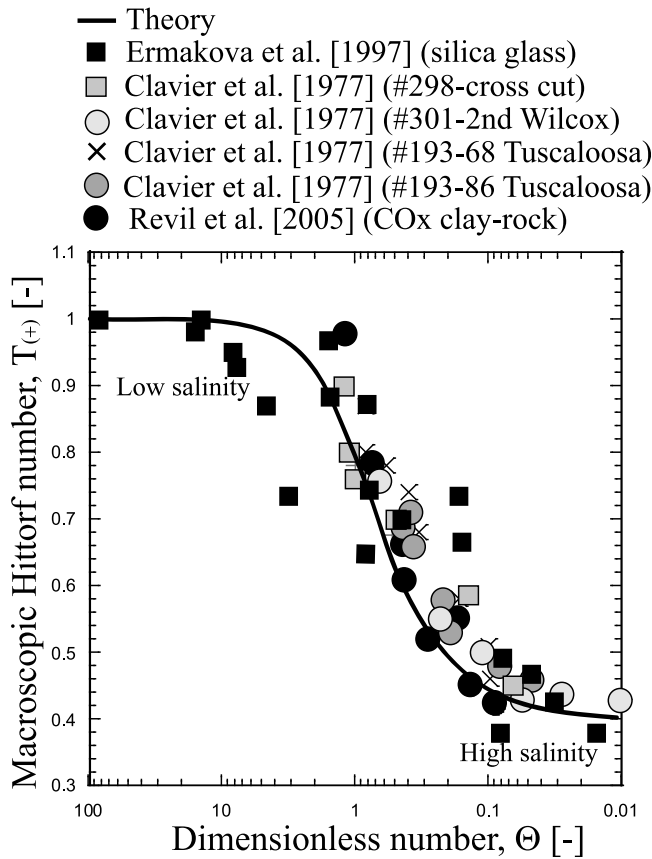


Figure 5. Hittorf number of the cations $T_{(+)}$ versus the dimensionless parameter Θ corresponding to the ratio of the diffuse layer counterion volumetric density divided by the salinity of a reservoir locally in equilibrium with the pore space. Experimental data are from (1) *Revil et al.* [2005, Figure 4b] (COx clay rock, NaCl), (2) *Clavier et al.* [1977] (shaley sands using the measured CEC and $f_Q = 0.90$, NaCl), and (3) *Ermakova et al.* [1997] (silica glass using the measured pore size and a surface charge density of 0.002 C m^{-2} , NaCl). The solid line represents the prediction from our theory. Correlation coefficient $R^2 = 0.87$.

We can check that if $\Theta \ll 1$ (high salinities), we have $\varepsilon = 0$ (no membrane behavior), while if $\Theta \gg 1$ (low salinities), we have $\varepsilon = 1$ (perfect membrane behavior). The behavior of ε versus Θ is shown in Figure 6. Our theory indicates that the osmotic efficiency should scale as $R C_f$, rather than as $R C_f^{1/2}$, as in the Bresler model [*Bresler*, 1973]. Note that the Bresler model has been strongly criticized recently by both *Neuzil and Provost* [2009] and *Rousseau-Gueutin et al.* [2010], both in terms of physical assumptions (equating the osmotic driving force with the hydraulic force) and in terms of the highly idealized nature of clay membranes. In order to compare our theory to experimental data, we first look for a simplified way to compute the dimensionless parameter Θ . Starting with the definition of this parameter (see equation (99)) and using the relationship between the volumetric charge density of the diffuse layer and the CEC (expressed in C kg^{-1}), we obtain

$$\Theta \equiv \frac{(1-f_Q)}{2eC_f} \rho_g \left(\frac{1-\phi}{\phi} \right) \text{CEC}. \quad (118)$$

This equation can be expressed as follows:

$$\Theta \equiv \frac{10^{-3}(1-f_Q)}{2C_f} \rho_g \left(\frac{1-\phi}{\phi} \right) \text{CEC}, \quad (119)$$

with C_f now expressed in molecules L^{-1} and the CEC in meq g^{-1} (we have used the following conversion: $1 \text{ meq g}^{-1} = N e \text{ C kg}^{-1} = 96,320 \text{ C kg}^{-1}$, where N is Avogadro's constant). A comparison between our model, equation (117), and various experimental data is reported in Figure 6. There is good agreement between the model and the experimental data. In each case, the CEC values are taken from published data or estimated depending on the composition of the clay fraction, and the fraction of counterions in the Stern layer is determined from the model of *Leroy and Revil* [2009].

[31] The last parameter we want to investigate is the mutual diffusion coefficient of a salt, like NaCl or KCl, through the COx clay rock in a salinity gradient. Using equation (87) with equation (79) for the expression of the conductivity contributions (without accounting for the Stern

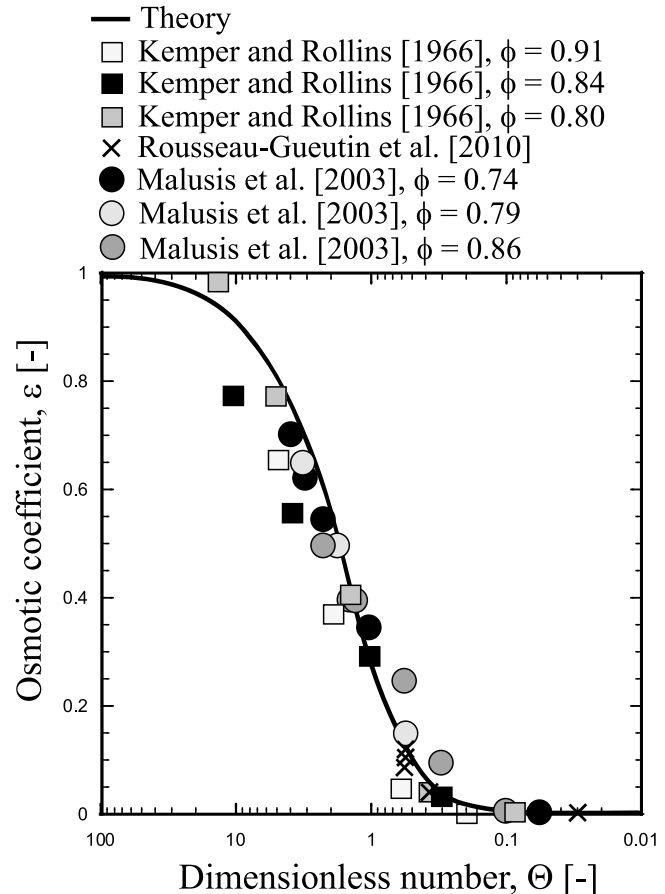


Figure 6. Osmotic coefficient ε versus the dimensionless parameter Θ . Experimental data are from (1) *Malusis et al.* [2003] (geosynthetic clay liner, KCl, $f_Q = 0.94$, measured CEC = 0.48 meq g^{-1} , $\rho_g = 2650 \text{ kg m}^{-3}$), (2) *Rousseau-Gueutin et al.* [2010, Table 4] (COx clay rock, NaCl), and (3) *Kemper and Rollins* [1966] (bentonite, $f_Q = 0.90$, NaCl, CEC = 0.8 meq g^{-1} , $\rho_g = 2650 \text{ kg m}^{-3}$). The solid line represents the prediction from our theory for KCl. Correlation coefficient $R^2 = 97$.

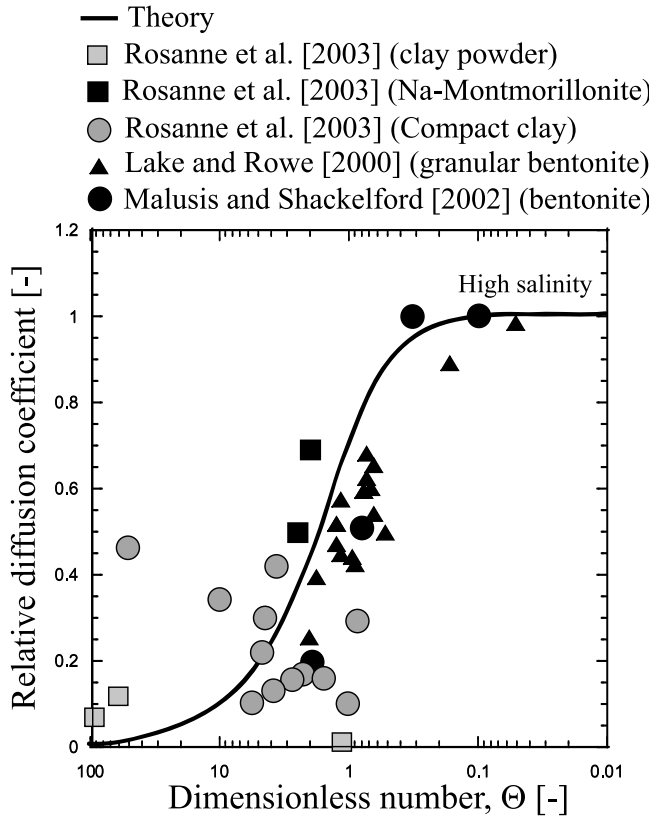


Figure 7. Relative diffusion coefficient γ versus the dimensionless parameter Θ . Experimental data are from (1) *Malusis and Shackelford* [2004] (geosynthetic clay liner, NaCl, $f_O = 0.94$, CEC = 0.48 meq g⁻¹, $\rho_g = 2650$ kg m⁻³, $D_f = 1.60 \times 10^{-9}$ m² s⁻¹), (2) *Lake and Rowe* [2000] (granular bentonite, NaCl, $f_O = 0.85$, CEC = 1.0 meq g⁻¹, $\rho_g = 2650$ kg m⁻³, $D_f = 1.60 \times 10^{-9}$ m² s⁻¹), (3) *Rosanne et al.* [2003, Table 5] (compact clay from the COx formation, NaCl, $f_O = 0.90$, CEC = 0.18 meq g⁻¹, $\rho_g = 2700$ kg m⁻³, $m = 2.5$, $D_f = 1.60 \times 10^{-9}$ m² s⁻¹), (4) *Rosanne et al.* [2003, Table 2] (Na-montmorillonite samples not free to swell, NaCl, $f_O = 0.90$, CEC = 0.8 meq g⁻¹, $\rho_g = 2650$ kg m⁻³, $m = 2.5$, $D_f = 1.60 \times 10^{-9}$ m² s⁻¹), and (5) *Rosanne et al.* [2003, Table 4] (clay powder from the COx formation, NaCl, $f_O = 0.90$, CEC = 0.18 meq g⁻¹, $\rho_g = 2700$ kg m⁻³, $m = 2.5$, $D_f = 1.60 \times 10^{-9}$ m² s⁻¹). The solid line represents the prediction from our theory. Correlation coefficient $R^2 = 0.55$.

layer contribution), the effective diffusion coefficient D (in m² s⁻¹) is given by

$$D = \frac{D_f}{F} \gamma. \quad (120)$$

In equation (120), D_f is the mutual diffusion coefficient of the salt in the reservoir (in m² s⁻¹),

$$D_f = \frac{2D_{(+)}^f D_{(-)}^f}{D_{(+)}^f + D_{(-)}^f}, \quad (121)$$

where $D_{(\pm)}^f = (k_b T / e) \beta_{(\pm)}$, according to the Nernst-Einstein relationship [see *Newman*, 1991; *Atkins*, 1998], $D_{(\pm)}^f$ are the

diffusion coefficients of the cations and anions in the reservoirs, and the correction coefficient γ (dimensionless) is given by

$$\gamma = \frac{(\beta_{(+)} + \beta_{(-)})}{\beta_{(+)}(\sqrt{1 + \Theta^2} + \Theta) + \beta_{(-)}(\sqrt{1 + \Theta^2} - \Theta)}, \quad (122)$$

$$\gamma \approx \frac{1}{\sqrt{1 + \Theta^2}}. \quad (123)$$

Because the ratio D_f/F represents the effective diffusion coefficient when the material is uncharged (or at very high salinities $\Theta \ll 1$), the correction coefficient γ can be seen as a normalized diffusion coefficient pointing out the effect of the diffuse layer upon the effective diffusion coefficient D . A comparison between our theory and various experimental data is shown in Figure 7. Note that the experimental data reported in Figure 7 have rather large error bars, which may explain some of the discrepancy between the model predictions and the data. The correction factor γ explains the discrepancy between the apparent diffusion coefficient and electrical formation factors for small porosities for clay and montmorillonite observed, for example, by *Rosanne et al.* [2003]. Therefore, our approach shows that the macroscopic mutual diffusion coefficient is controlled by the electrical formation factor, but a correction term needs to be accounted for. This correction term depends on the ratio Θ .

[32] Before we conclude, we need to explain why the transport properties above are better explained without considering the Stern layer contribution. A major difference between our model and the microstructure of the investigated porous media is related to the continuity of the solid phase. In true porous media, the discontinuity of the solid phase implies the discontinuity of the Stern layer. As long as the frequency of the excitation is below a certain frequency, the electromigration current density of the Stern layer is counterbalanced by the diffusion current density. This is consistent with our finding that the Stern layer polarizes only above a certain frequency range associated with the grain size distribution [*Leroy et al.*, 2008; *Revil and Florsch*, 2010; *Vaudelet et al.*, 2011].

4. Concluding Statements

[33] We have developed a set of constitutive equations describing transport phenomena in charged porous rocks. These constitutive equations are coupled to each other through a variety of mechanisms, mostly related to the existence of the electrical double layer at the pore water-mineral interface. The originality of this new model is that it accounts for the pore size distribution and potential migration (diffusion and electromigration) in the Stern layer of weakly sorbed counterions along the mineral surface. This means that the present model can be easily extended to the frequency domain to investigate induced polarization phenomena. The partition of the counterions and coions between the Stern and diffuse layers helps to resolve a number of discrepancies observed between classical theories and experimental data, especially when dealing with induced polarization data. We found, however, no experimental evidence for this transport mechanism in the quasi-static

case. This is consistent with the work done on modeling induced polarization in porous media showing no contribution of the Stern layer to the DC surface conductivity of granular media [Vaudelet *et al.*, 2011]. The contribution of the Stern layer cannot be neglected above 0.1 mHz in sands, for instance [Revil and Florsch, 2010].

[34] Under the condition that the Stern layer does not contribute to quasi-static transport properties, the cross-coupled material properties are controlled by the dimensionless number Θ , which is the ratio of the volumetric charge density of the diffuse layer to the salinity of a fictitious neutral reservoir locally in equilibrium with the pore space of the porous material.

[35] The present approach can be also easily generalized to the case of pores of different shapes by defining families of pores with different cross-sectional geometries (e.g., parallel plates for modeling microcracks in addition to cylindrical cores). It can also be generalized to the case where several minerals are present by defining families of pore size distributions embedded into different minerals. Finally, using the approach of Revil and Linde [2006], it could be generalized to a multicomponent electrolyte. To be complete, the present modeling also needs to be associated with the macroscopic mass and charge balance equations.

[36] Our model does not account for the connectivity between the pores, and further work will be needed to include the connectivity of material properties, as well the connectivity of the solid phase. The present work also constitutes a fundamental step toward developing a complete set of constitutive equations in unsaturated porous media (for vadose zone applications) or for multiphase flow problems, including gas, oil, and water in oil and gas reservoirs. We plan to develop such a theory, incorporating the influence of the pore size distribution derived from the capillary pressure curve and/or NMR data. Connectivity will also be included to model hysteretic effects.

Appendix A: Donnan Model and Osmotic Pressure

[37] In this appendix, we first derive the expression of the concentration in the pore space of a porous material using the Donnan approach. We then retrieve classical expressions for the osmotic pressure in a fictitious reservoir in local equilibrium with the pore space of the porous material (at each point). The ionic concentration in the (neutral) fictitious reservoir of ions is $C_{(\pm)} = C_f$. The expressions of the electrochemical potentials of the cations and anions in the fictitious reservoir and in the pore space are [e.g., Helfferich, 1995]

$$\tilde{\mu}_{(\pm)} = \mu_{(\pm)}^0 + k_b T \ln C_{(\pm)} \pm e\psi, \quad (\text{A1})$$

$$\bar{\mu}_{(\pm)} = \mu_{(\pm)}^0 + k_b T \ln \bar{C}_{(\pm)} \pm e(\psi + \bar{\varphi}), \quad (\text{A2})$$

respectively. The overbar is used to express that the quantity is considered in the pore space. In these expressions, $\bar{\varphi}$ is the mean (microscopic) electrical potential distribution associated with the electrical diffuse layer in the capillary ($\bar{\varphi} = 0$ in the reservoir). Thermodynamic equilibrium between the fictitious reservoir and the pore space implies

$$\bar{\mu}_{(\pm)} = \tilde{\mu}_{(\pm)}, \quad (\text{A3})$$

which leads directly to Boltzmann distributions for the concentrations of the cations and anions in the pore space of the charged material. The charge conservation equation can be written as equation (74). Solving these equations yields well-known expressions for the ionic concentrations in the pore space of the material and an expression for the mean electrostatic potential [Teorell, 1935; Meyer and Sievers, 1936],

$$\bar{C}_{(\pm)} = C_f \left(\sqrt{1 + \Theta^2} \pm \Theta \right), \quad (\text{A4})$$

$$\Theta \equiv \frac{Q_S}{eC_f} \frac{\Pi_1}{\Pi_2}, \quad (\text{A5})$$

$$\bar{\varphi} = -\frac{k_b T}{2e} \ln \left[\frac{\sqrt{1 + \Theta^2} + \Theta}{\sqrt{1 + \Theta^2} - \Theta} \right], \quad (\text{A6})$$

which corresponds to the Donnan model. The potential $\bar{\varphi}$ is the mean electrostatic potential of the porous material as a whole and is different from the mean electrostatic potential in each capillary. The only difference between the original Teorell-Sievers-Meyer (TMS) model and our approach is that our approach is generalized to a pore size distribution, while the TMS model considers a single pore size.

[38] The osmotic pressure in a reservoir and the chemical potential of the water in this reservoir are given by [Kedem and Katchalsky, 1958]

$$\pi = -\frac{k_b T}{\Omega_w} \ln C_w = -\frac{k_b T}{\Omega_w} \ln(1 - 2\Omega_f C_f) \approx 2k_b T C_f, \quad (\text{A7})$$

$$\mu_w = \mu_w^0 + \Omega_w p + k_b T \ln C_w, \quad (\text{A8})$$

respectively, where p is the mechanical pressure. Therefore, the chemical potential of the water in the reservoir can be written as

$$\mu_w = \mu_w^0 + \Omega_w (p - \pi), \quad (\text{A9})$$

and the chemical potential gradient in water is

$$\nabla \mu_w = \Omega_w \nabla (p - \pi), \quad (\text{A10})$$

where $p^* = p - \pi$ represents the total (effective) fluid pressure. The Stokes equation, which is a momentum conservation equation, is traditionally written for pure water. It needs to be modified to account for the presence of ions as discussed in the text (see equation (3)). Similarly, the chemical potential of the water in the pore space of the material is

$$\bar{\pi} = -\frac{k_b T}{\Omega_w} \ln \bar{C}_w, \quad (\text{A11})$$

$$\bar{\mu}_w = \mu_w^0 + \Omega_w \bar{p} + k_b T \ln \bar{C}_w, \quad (\text{A12})$$

where \bar{C}_w and \bar{p} are the water concentration and internal fluid pressure in the pore space of the porous material, respectively (we have assumed ideality, and therefore,

activities and concentrations are equal). We can also write the chemical potential of water in the pore space as

$$\bar{\mu}_w = \mu_w^0 + \Omega_w(\bar{p} - \bar{\pi}). \quad (\text{A13})$$

The conservation of mass in the reservoir and in the pore space can be described as

$$\Omega_w C_w + (\Omega_{(+)} + \Omega_{(-)}) C_f = 1, \quad (\text{A14})$$

$$\Omega_w \bar{C}_w + \Omega_{(+)} \bar{C}_{(+)} + \Omega_{(-)} \bar{C}_{(-)} = 1, \quad (\text{A15})$$

respectively. Local thermodynamic equilibrium between the fictitious reservoir and the pore water implies

$$\bar{\mu}_w = \mu_w. \quad (\text{A16})$$

Equations (A7)–(A16) yield the following expression for the internal pore pressure in the charged porous material:

$$\bar{p} = p - (\pi - \bar{\pi}). \quad (\text{A17})$$

The difference of osmotic pressure between the reservoir and the pore water is

$$\delta\pi = \pi - \bar{\pi} = -\frac{k_b T}{\Omega_w} \ln\left(\frac{C_w}{\bar{C}_w}\right), \quad (\text{A18})$$

$$\delta\pi = -\frac{k_b T}{\Omega_w} \ln\left(\frac{1 - 2\Omega_w C_f}{1 - \Omega_w \bar{C}_{(+)} - \Omega_w \bar{C}_{(-)}}\right), \quad (\text{A19})$$

$$\delta\pi \approx -k_b T (\bar{C}_{(+)} + \bar{C}_{(-)} - 2C_f), \quad (\text{A20})$$

where we have used a first-order Taylor expansion of the argument of the logarithm and assumed that the molar volume of the different molecules are roughly the same. Starting with the definitions of the osmotic pressures, equations (A7) and (A11), and using the mass conservation equations, we can also obtain the following expressions for the osmotic pressure in the reservoir and for the osmotic pressure in the pore space of the porous material:

$$\pi = k_b T (2C_f), \quad (\text{A21})$$

$$\bar{\pi} = k_b T (\bar{C}_{(+)} + \bar{C}_{(-)}), \quad (\text{A22})$$

where equation (A21) is the classical *van't Hoff* [1888] equation (also called the Morse equation) in a neutral electrolyte, while equation (A22) is an extension of this equation for the pore space of a charge porous material. We can also express the difference in osmotic pressure between the reservoir and the local pore space as a function of the mean potential or as a function of the key dimensionless variable Θ :

$$\delta\pi = -2C_f k_b T \left[\cosh\left(\frac{e\bar{\varphi}}{k_b T}\right) - 1 \right], \quad (\text{A23})$$

$$\delta\pi = -2C_f k_b T \left(\sqrt{1 + \Theta^2} - 1 \right). \quad (\text{A24})$$

Similarly, the osmotic pressure in the pore space can be written as

$$\bar{\pi} = 2C_f k_b T \cosh\left(\frac{e\bar{\varphi}}{k_b T}\right). \quad (\text{A25})$$

This is consistent with the integration of the excess of charge with respect to the mean potential. Indeed,

$$\delta\pi = \int_0^{\bar{\varphi}} \bar{Q}_V d\bar{\varphi}', \quad (\text{A26})$$

$$\delta\pi = e \int_0^{\bar{\varphi}} (\bar{C}_{(+)} - \bar{C}_{(-)}) d\bar{\varphi}', \quad (\text{A27})$$

$$\delta\pi = -2C_f k_b T \left[\cosh\left(\frac{e\bar{\varphi}}{k_b T}\right) - 1 \right], \quad (\text{A28})$$

$$\delta\pi = \pi - \bar{\pi}. \quad (\text{A29})$$

Equation (A26) is, for instance, discussed by *Gonçalvès et al.* [2010] in terms of the electrostatic contribution to the disjoining pressure. In going from equation (A27) to equation (A28), we have used the Boltzmann distributions discussed at the beginning of this appendix. The pressure difference $\delta\pi$ is the difference in osmotic pressure between the osmotic pressure of the reservoir and the osmotic pressure of the pore water, and this difference arises because of the electrostatic force inside the pore space of the charged material.

[39] We now turn our attention to the local flux densities of ions. These fluxes are related to the ionic concentrations and to the drift velocity by [*Cussler, 1997*]

$$\mathbf{j}_{(\pm)} = \bar{C}_{(\pm)} \mathbf{v}. \quad (\text{A30})$$

The velocity \mathbf{v} can be divided into three components, including a mechanical, an electrical, and a diffusional contribution ($\mathbf{v} = \mathbf{v}_m + \mathbf{v}_e + \mathbf{v}_c$). Therefore, the flux densities are given by

$$\mathbf{j}_{(\pm)} = \bar{C}_{(\pm)} \mathbf{v}_c + \bar{C}_{(\pm)} \mathbf{v}_e + \bar{C}_{(\pm)} \mathbf{v}_m, \quad (\text{A31})$$

$$\mathbf{v}_c = -b_{(\pm)} \nabla \mu_{(\pm)}, \quad (\text{A32})$$

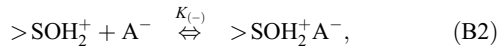
$$\mathbf{v}_e = (\pm 1) \beta_{(\pm)} \mathbf{E}, \quad (\text{A33})$$

where $b_{(\pm)}$ (in $\text{m}^2 \text{s}^{-1} \text{J}^{-1}$) and $\beta_{(\pm)}$ (in $\text{m}^2 \text{s}^{-1} \text{V}^{-1}$) are the two mobilities described in the text, defining the drift velocity for diffusion and electromigration, respectively [see *Newman, 1991; Atkins, 1998*], and $\mu_{(\pm)}$ are the chemical potentials of the cations and anions. Equations (A31)–(A33) yield the so-called Nernst-Planck equation.

Appendix B: Sorption and Transport in the Stern Layer

[40] In order to gain better insight into transport in the Stern layer, we introduce the microscopic equations

describing the physics of the transport of counterions and coions located in the Stern layer. The existence of the Stern layer comprising weakly sorbed counterions on the mineral surface is, for example, demonstrated by molecular dynamic simulations [Tournassat *et al.*, 2009]. To simplify our analysis, we consider the sorption of coions and counterions at the surface of silica [see Li and de Bruyn, 1966], but the final results are very general. We consider the following sorption reactions [e.g., Wang and Revil, 2010]:



where $>SOH$ represents a surface hydroxyl site and $K_{(\pm)}$ are the sorption constants. The sorption of the coions A^- and counterions M^+ are therefore governed by [Wang and Revil, 2010]

$$K_{(+)} = \frac{\Gamma_{(+)}}{\Gamma_{(-)}^0 C_{(+)} \exp\left(-\frac{e\phi_d}{k_b T}\right)}, \quad (B3)$$

$$K_{(-)} = \frac{\Gamma_{(-)}}{\Gamma_{(+)}^0 C_{(-)} \exp\left(\frac{e\phi_d}{k_b T}\right)}, \quad (B4)$$

where $\Gamma_{(+)}$ and $\Gamma_{(-)}$ represent the density of surface species $>SO^-M^+$ and $>SOH_2^+A^-$ (in m^{-2}), respectively, and $\Gamma_{(-)}^0$ and $\Gamma_{(+)}^0$ represent the density of surface species $>SO^-$ and $>SOH_2^+$ surface species (in m^{-2}), respectively. The fluxes of counterions and coions along the mineral surface are given by an interfacial version of the Nernst-Planck local equation as suggested by Zukoski and Saville [1986a, 1986b]:

$$\mathbf{j}_{(\pm)} = -b_{(\pm)}^S \Gamma_{(\pm)} \nabla_S \tilde{\mu}_{(\pm)}^S, \quad (B5)$$

$$\mathbf{j}_{(\pm)} = -b_{(\pm)}^S \Gamma_{(\pm)} \nabla_S [(\pm e)\psi + k_b T \ln \Gamma_{(\pm)}], \quad (B6)$$

$$\mathbf{j}_{(\pm)} = -b_{(\pm)}^S \Gamma_{(\pm)} (\pm e) \nabla_S \psi - k_b T b_{(\pm)}^S \Gamma_{(\pm)} \nabla_S \ln \Gamma_{(\pm)}, \quad (B7)$$

where $\tilde{\mu}_{(\pm)}^S$ denotes the electrochemical potential along the mineral surface (in J), ∇_S denotes a surface gradient along the mineral surface, and $(\pm 1)e$ is the charge of counterions and coions (in C). The potential tangential mobility of the weakly sorbed counterions at the surface of silica is confirmed by nuclear magnetic resonance (NMR) spectroscopy. For instance, in the case of sodium on silica, Carroll *et al.* [2002] showed that sodium forms a mobile outer-sphere surface complex on the basis of the narrow line width of the NMR spectra, the lack of chemical shift from aqueous sodium, and negligible quadrupolar couplings.

[41] We come back to the transport problem at a scale of a capillary shown in Figure 1. From equations (B3) and (B4), we have

$$\nabla_S \ln \Gamma_{(\pm)} = \nabla_S \ln C_{(\pm)}; \quad (B8)$$

therefore, the surface gradients of the logarithm of the surface densities of counterions and coions are equal to the

surface gradients of the logarithm of the bulk concentrations. For a capillary, the surface gradient is equal to the bulk gradient, and therefore, the surface fluxes of counterions and coions are given by

$$\mathbf{j}_{(\pm)} = -b_{(\pm)}^S \Gamma_{(\pm)} (\pm e) \nabla \psi - k_b T b_{(\pm)}^S \Gamma_{(\pm)} \nabla \ln C_{(\pm)}, \quad (B9)$$

$$\mathbf{j}_{(\pm)} = -b_{(\pm)}^S \Gamma_{(\pm)} \nabla \tilde{\mu}_{(\pm)}^S, \quad (B10)$$

and therefore, the flux of species along the mineral surface is controlled by the gradient of the macroscopic electrochemical potential between the two reservoirs.

Appendix C: Scaling Laws

[42] We first investigate the scaling between the electrical conductivity and the raw moments of the pore size distribution. Let's consider a single capillary i . The current density J_i is given by the local Ohm's law,

$$J_i = \frac{I_i}{A_i} = \bar{\sigma}_f \frac{\Delta\psi}{L} + \frac{2\pi R_i}{\pi R_i^2} \Sigma_S \frac{\Delta\psi}{L}, \quad (C1)$$

where I_i and A_i are the current and surface area of a cross section of the capillary, respectively, $\Delta\psi/L$ is the electrical field, R_i is the radius of the capillary, and L is its length. The total current I for a collection of n capillaries is defined as the sum of all the currents through all the capillaries (fluxes are cumulative):

$$I = \sum_{i=1}^n I_i = \sum_{i=1}^n (\bar{\sigma}_f A_i + 2R_i \Sigma_S) \frac{\Delta\psi}{L}. \quad (C2)$$

The total (macroscopic) current density of the porous material is therefore given by

$$J = \frac{I}{A} = \frac{1}{A} \sum_{i=1}^n (\bar{\sigma}_f A_i + 2R_i \Sigma_S) \frac{\Delta\psi}{L}, \quad (C3)$$

$$J = \left[\bar{\sigma}_f \phi + \frac{1}{A} \left(\sum_{i=1}^n 2R_i \right) \Sigma_S \right] \frac{\Delta\psi}{L}, \quad (C4)$$

$$J = \phi \left[\bar{\sigma}_f + 2 \left(\frac{\sum_{i=1}^n R_i}{\sum_{i=1}^n R_i^2} \right) \Sigma_S \right] \frac{\Delta\psi}{L}, \quad (C5)$$

$$J = \phi \left(\bar{\sigma}_f + 2 \frac{\Pi_1}{\Pi_2} \Sigma_S \right) \frac{\Delta\psi}{L}. \quad (C6)$$

As J is also given by a macroscopic Ohm's law and assuming that the capillaries are characterized by a certain tortuosity $F\phi$, the electrical conductivity of the porous material is given by

$$\sigma = \frac{1}{F} \left(\bar{\sigma}_f + 2 \frac{\Pi_1}{\Pi_2} \Sigma_S \right). \quad (C7)$$

We focus now on the scaling between the volumetric excess of charge and the raw moments of the pore size distribution. For a single capillary i , the local volumetric charge density

\bar{q}_V^i (averaged over the pore space of the capillary) is related to the effective surface charge density Q_S on the surface of the walls of the capillary by

$$\bar{q}_V^i = -2Q_S \frac{1}{R_i}. \quad (C8)$$

In equation (C8), the factor $2/R_i$ corresponds to the surface per pore volume ratio. If N_i represents the number of charges in excess to neutrality in the capillary i , we also have

$$\bar{q}_V^i = \frac{N_i}{V_p^i}, \quad (C9)$$

where V_p^i is the volume of the capillary i . For a collection of n capillaries, the volumetric charge density of the porous material is defined by

$$\bar{Q}_V = \frac{1}{V_p} \sum_{i=1}^n N_i = \frac{-2\pi L Q_S \sum_{i=1}^n R_i}{L\pi \sum_{i=1}^n R_i^2}, \quad (C10)$$

where V_p is the total pore volume (therefore, the total number of excess charge is cumulative). We can rewrite equation (C10) in terms of the raw moments of the pore size distribution,

$$\bar{Q}_V = -2Q_S \frac{\Pi_1}{\Pi_2}. \quad (C11)$$

We observe, therefore, that surface conductivity in equation (C7) and the volumetric charge density share the same scaling law.

[43] We look now at the streaming current. For a single capillary, we have

$$J_i = \frac{I_i}{A_i} = \bar{q}_V \frac{R_i^2}{8\eta} \frac{\Delta p}{L}. \quad (C12)$$

For a collection of n capillaries and following the chain rules as previously, we find

$$J = \tilde{Q}_V U, \quad (C13)$$

$$\tilde{Q}_V = \bar{Q}_V \frac{\Pi_2 \Pi_3}{\Pi_4 \Pi_1} \leq \bar{Q}_V. \quad (C14)$$

$\tilde{Q}_V \approx \bar{Q}_V$ is obtained only with the additional assumption that $\Pi_2 \Pi_3 \approx \Pi_4 \Pi_1$.

Appendix D: Permeability and Electrical Conductivity

[44] According to our model, the effective electrical conductivity can be written as

$$\sigma = \frac{1}{F} \left(\bar{\sigma}_f + \frac{2}{\Lambda} \Sigma_S \right), \quad (D1)$$

where Λ (in m) is a characteristic length scale, termed the effective or dynamic pore radius [Johnson and Sen, 1988]. In a real porous material, equation (D1) is only valid at high salinities (see discussion of Bernabé and Revil [1995]). Pride [1994] developed an equation similar to equation (D1) with two differences: (1) in the model of Pride [1994], the

surface conductivity term is due to the diffuse layer only (there is no contribution from the Stern layer in his model), and (2) in Pride's [1994] model, the conductivity of the pore water is equal to the conductivity of the pore water in a reservoir in local equilibrium with the porous material. This is not the case in our model because of the influence of the diffuse layer in the pore space ($\bar{\sigma}_f \neq \sigma_f$). A comparison between equation (83) and equation (D1) yields

$$\frac{1}{\Lambda} = \frac{\Pi_1}{\Pi_2}. \quad (D2)$$

This result is strictly true only for the capillary model investigated in the present paper. The applicability of this relationship to real media should be investigated further.

[45] A number of researchers [see Banavar and Johnson, 1987; Johnson and Sen, 1988; Pride, 1994; Revil and Cathles, 1999, and references therein] have proposed the following relationship between the permeability, the formation factor, and the length scale Λ :

$$k = \frac{\Lambda^2}{8F}. \quad (D3)$$

Equations (D2) and (D3) imply

$$k \approx \frac{1}{8F} \left(\frac{\Pi_1}{\Pi_2} \right)^2. \quad (D4)$$

The correct equation for the permeability of a bundle of capillaries is given by equation (72) of the main text. Therefore, equation (D4) is accurate only if the following approximation is valid:

$$\left(\frac{\Pi_1}{\Pi_2} \right)^2 \approx \frac{\Pi_2}{\Pi_4}. \quad (D5)$$

We plan to investigate in a future contribution under what circumstances this approximation is expected to hold.

[46] **Acknowledgments.** We thank the National Science Foundation (NSF award CMMI 0926276) and the Office of Science (BER), U.S. Department of Energy (award DE-FG02-08ER646559), for financial support. We thank Niklas Linde, two additional anonymous referees, and the Associate Editor for their very constructive comments. We thank referee 1 for helping us derive the conductivity expression for a collection of capillaries. A.R. thanks Lynn Bennethum for fruitful discussions.

References

- Agence Nationale pour la Gestion des Déchets Radioactifs (2005), Dossier 2005 argile-Référentiel du site de Meuse/Haute Marne, *Internal Rep. ANDRA C.RP.ADS.04.0022*, Châtenay-Malabry, France.
- Archie, G. E. (1942), The electrical resistivity log as an aid in determining some reservoir characteristics, *Trans. Am. Inst. Min. Metall. Pet. Eng.*, 146, 54–62.
- Atkins, P. (1998), *Physical Chemistry*, 6th ed., Oxford Univ. Press, Oxford, U. K.
- Auriault, J.-L., and J. Lewandowska (1993), Homogenization analysis of diffusion and adsorption macrotransport in porous media: Macrotransport in the absence of advection, *Geotechnique*, 43(3), 457–469, doi:10.1680/geot.1993.43.3.457.
- Banavar, J. R., and D. L. Johnson (1987), Characteristic pore sizes and transport in porous media, *Phys. Rev. B*, 35, 7283–7286, doi:10.1103/PhysRevB.35.7283.
- Bennethum, L. S., and J. H. Cushman (2002a), Multicomponent, multiphase thermodynamics of swelling porous media with quasillectrostatics: I. Macroscale field equations, *Transp. Porous Media*, 47, 309–336, doi:10.1023/A:1015558130315.

- Bennethum, L. S., and J. H. Cushman (2002b), Multicomponent, multiphase thermodynamics of swelling porous media with quasidelectrostatics: II. Constitutive theory, *Transp. Porous Media*, *47*, 337–362, doi:10.1023/A:1015562614386.
- Bernabé, Y. (1998), Streaming potential in heterogeneous networks, *J. Geophys. Res.*, *103*, 20,827–20,841, doi:10.1029/98JB02126.
- Bernabé, Y., and A. Revil (1995), Pore-scale heterogeneity, energy dissipation and the transport properties of rocks, *Geophys. Res. Lett.*, *22*, 1529–1552, doi:10.1029/95GL01418.
- Binley, A., L. D. Slater, M. Fukes, and G. Cassiani (2005), Relationship between spectral induced polarization and hydraulic properties of saturated and unsaturated sandstones, *Water Resour. Res.*, *41*, W12417, doi:10.1029/2005WR004202.
- Bresler, E. (1973), Anion exclusion and coupling effects in non-steady transport through unsaturated soils: I. Theory, *Soil Sci. Soc. Am. Proc.*, *37*(5), 663–669, doi:10.2136/sssaj1973.03615995003700050013x.
- Bussian, A. E. (1983), Electrical conductance in a porous medium, *Geophys. Res.*, *88*, 1258–1268, doi:10.1190/1.1441549.
- Carroll, S., R. S. Maxwell, W. Bourcier, S. Martin, and S. Hulsey (2002), Evaluation of silica-water surface chemistry using NMR spectroscopy, *Geochim. Cosmochim. Acta*, *66*, 913–926, doi:10.1016/S0016-7037(01)00827-4.
- Cervera, J., P. Ramirez, J. A. Manzanares, and S. Mafé (2010), Incorporating ionic size in the transport equations for charged nanopores, *Microfluid. Nanofluid.*, *9*, 41–53, doi:10.1007/s10404-009-0518-2.
- Clavier, C., G. Coates, and J. Dumanoir (1977), The theoretical and experimental bases for the “dual water” model for the interpretation of shaly sands, paper SPE 6869 presented at 52nd Annual Fall Technical Conference and Exhibition of the Society of Petroleum Engineers of AIME, Denver, Colo., 9–12 Oct.
- Cosenza, P., A. Ghorbani, C. Camerlynck, F. Rejiba, R. Guérin, and A. Tabbagh (2009), Effective medium theories for modeling the relationships between electromagnetic properties and hydrological variables: A review, *Near Surf. Geophys.*, *7*, 563–578.
- Cussler, E. (1997), *Diffusion: Mass Transfer in Fluid Systems*, 2nd ed., Cambridge Univ. Press, Cambridge, U. K.
- de Groot, D. V., and P. Mazur (1984), *Non-equilibrium Thermodynamics*, Dover, New York.
- Delay, J., and M. Distinguin (2004), Hydrogeological investigations in deep wells at the Meuse/Haute Marne Underground Research Laboratory, in *Engineering Geology for Infrastructure Planning in Europe*, *Lect. Notes Earth Sci.*, vol. 104, edited by R. Hack, R. Azzam, and R. Charlier, pp. 219–225, Springer, Berlin.
- Descostes, M., V. Blin, F. Bazer-Bachi, P. Meier, B. Grenut, J. Radwan, M. L. Schlegel, S. Buschaert, D. Coelho, and E. Tevissen (2008), Diffusion of anionic species in Callovo-Oxfordian argillites and Oxfordian limestones (Meuse/Haute-Marne, France), *Appl. Geochem.*, *23*, 655–677, doi:10.1016/j.apgeochem.2007.11.003.
- Distinguin, M., and J.-M. Lavanchy (2007), Determination of hydraulic properties of the Callovo-Oxfordian argillite at the Bure site: Synthesis of the results obtained in deep boreholes using several in situ investigation techniques, *Phys. Chem. Earth*, *32*, 379–392.
- Dormieux, L. (2005), A mathematical framework for upscaling operations, in *Applied Micromechanics of Porous Materials*, *CISM Ser.*, vol. 480, edited by P. Dormieux and F. Ulm, pp. 109–152, Springer, New York.
- Dullien, F. A. L. (1992), *Porous Media: Fluid Transport and Pore Structure*, 2nd ed., 574 pp., Academic, San Diego, Calif.
- Ermakova, L. E., M. Sidorova, N. Jura, and I. Savina (1997), Adsorption and electrokinetic characteristics of micro- and macroporous glasses in 1:1 electrolytes, *J. Membr. Sci.*, *131*, 125–141, doi:10.1016/S0376-7388(97)00036-7.
- Fritz, S. J. (1986), Ideality of clay membranes in osmotic processes: A review, *Clays Clay Miner.*, *34*, 214–223, doi:10.1346/CCMN.1986.0340212.
- Furini, S., F. Zerbetto, and S. Cavalcanti (2006), Application of the Poisson-Nernst-Planck theory with space-dependent diffusion coefficients to KcsA, *Biophys. J.*, *91*(9), 3162–3169, doi:10.1529/biophysj.105.078741.
- Gaucher, E., et al. (2004), ANDRA underground research laboratory: Interpretation of the mineralogical and geochemical data acquired in the Callovo-Oxfordian Formation by investigative drilling, *Phys. Chem. Earth*, *29*, 55–77, doi:10.1016/j.pce.2003.11.006.
- Gaucher, E., et al. (2006), Modeling the pore water chemistry of the Callovo-Oxfordian formation at a regional scale, *C. R. Geosci.*, *338*(12–13), 917–930, doi:10.1016/j.crte.2006.06.002.
- Gonçalves, J., P. Rousseau-Gueutin, and A. Revil (2007), Introducing interacting diffuse layers in TLM calculations: A reappraisal of the influence of the pore size on the swelling pressure and the osmotic efficiency of compacted bentonites, *J. Colloid Interface Sci.*, *316*, 92–99, doi:10.1016/j.jcis.2007.07.023.
- Gonçalves, J., P. Rousseau-Gueutin, G. de Marsily, P. Cosenza, and S. Violette (2010), What is the significance of pore pressure in a saturated shale layer?, *Water Resour. Res.*, *46*, W04514, doi:10.1029/2009WR008090.
- Gray, W. G., and S. M. Hassanizadeh (1991), Unsaturated flow theory including interfacial phenomena, *Water Resour. Res.*, *27*(8), 1855–1863, doi:10.1029/91WR01260.
- Helferich, F. (1995), *Ion Exchange*, Dover, New York.
- Ishido, T., and H. Mizutani (1981), Experimental and theoretical basis of electrokinetic phenomena in rock-water systems and its applications in geophysics, *J. Geophys. Res.*, *86*, 1763–1775, doi:10.1029/JB086iB03p01763.
- Jackson, M. D. (2008), Characterization of multiphase electrokinetic coupling using a bundle of capillary tubes model, *J. Geophys. Res.*, *113*, B04201, doi:10.1029/2007JB005490.
- Jackson, M. D. (2010), Multiphase electrokinetic coupling: Insights into the impact of fluid and charge distribution at the pore scale from a bundle of capillary tubes model, *J. Geophys. Res.*, *115*, B07206, doi:10.1029/2009JB007092.
- Jardani, A., A. Revil, A. Bolève, J. P. Dupont, W. Barrash, and B. Malama (2007), Tomography of the Darcy velocity from self-potential measurements, *Geophys. Res. Lett.*, *34*, L24403, doi:10.1029/2007GL031907.
- Jardani, A., A. Revil, E. Slob, and W. Sollner (2010), Stochastic joint inversion of 2D seismic and seismoelectric signals in linear poroelastic materials, *Geophysics*, *75*, N19–N31, doi:10.1190/1.3279833.
- Johnson, D. L., and P. N. Sen (1988), Dependence of the conductivity of a porous medium on electrolyte conductivity, *Phys. Rev. B*, *37*, 3502–3510, doi:10.1103/PhysRevB.37.3502.
- Jougnot, D., A. Revil, and P. Leroy (2009), Diffusion of ionic tracers in the Callovo-Oxfordian clay-rock using the Donnan equilibrium model and the electrical formation factor, *Geochim. Cosmochim. Acta*, *73*, 2712–2726, doi:10.1016/j.gca.2009.01.035.
- Jougnot, D., A. Revil, N. Lu, and A. Wayllace (2010a), Transport properties of the Callovo-Oxfordian clay rock under partially saturated conditions, *Water Resour. Res.*, *46*, W08514, doi:10.1029/2009WR008552.
- Jougnot, D., A. Ghorbani, A. Revil, P. Leroy, and P. Cosenza (2010b), Spectral induced polarization of partially saturated clay-rocks: A mechanistic approach, *Geophys. J. Int.*, *180*, 210–224, doi:10.1111/j.1365-246X.2009.04426.x.
- Kedem, O., and A. Katchalsky (1958), Thermodynamics analysis of the permeability of biological membranes to non-electrolytes, *Biochim. Biophys. Acta*, *27*, 229–246, doi:10.1016/0006-3002(58)90330-5.
- Kemna, A., A. Binley, A. Ramirez, and W. Daily (2000), Complex resistivity tomography for environmental applications, *Chem. Eng. J.*, *77*, 11–18, doi:10.1016/S1385-8947(99)00135-7.
- Kemper, W. D., and J. B. Rollins (1966), Osmotic efficiency coefficients across compacted clays, *Soil Sci. Soc. Am. Proc.*, *30*(5), 529–534, doi:10.2136/sssaj1966.03615995003000050005x.
- Knight, R., et al. (2010), Geophysics at the interface: The response of geophysical properties to solid-fluid, fluid-fluid, and solid-solid interfaces, *Rev. Geophys.*, *48*, RG4002, doi:10.1029/2007RG000242.
- Lake, C. B., and R. K. Rowe (2000), Diffusion of sodium and chloride through geosynthetic clay liners, *Geotext. Geomembr.*, *18*(2–4), 103–131, doi:10.1016/S0266-1144(99)00023-0.
- Leinov, E., J. Vinogradov, and M. D. Jackson (2010), Salinity dependence of the thermoelectric coupling coefficient in brine-saturated sandstones, *Geophys. Res. Lett.*, *37*, L23308, doi:10.1029/2010GL045379.
- Leroy, P., and A. Revil (2009), A mechanistic model for the spectral induced polarization of clay materials, *J. Geophys. Res.*, *114*, B10202, doi:10.1029/2008JB006114.
- Leroy, P., A. Revil, S. Altmann, and C. Tourmassat (2007), Modeling the composition of the pore water in a clay-rock geological formation (Callovo-Oxfordian, France), *Geochim. Cosmochim. Acta*, *71*, 1087–1097, doi:10.1016/j.gca.2006.11.009.
- Leroy, P., A. Revil, A. Kemna, P. Cosenza, and A. Gorbani (2008), Spectral induced polarization of water-saturated packs of glass beads, *J. Colloid Interface Sci.*, *321*, 103–117, doi:10.1016/j.jcis.2007.12.031.
- Li, H., and P. L. de Bruyn (1966), Electrokinetic and adsorption studies on quartz, *Surf. Sci.*, *5*(2), 203–220, doi:10.1016/0039-6028(66)90082-3.
- Linde, N. (2009), Comment on “Characterization of multiphase electrokinetic coupling using a bundle of capillary tubes model” by Mathew D. Jackson, *J. Geophys. Res.*, *114*, B06209, doi:10.1029/2008JB005845.
- Malusis, M. A., and C. D. Shackelford (2004), Predicting solute flux through a clay membrane barrier, *J. Geotech. Geoenviron. Eng.*, *130*(5), 477–487, doi:10.1061/(ASCE)1090-0241(2004)130:5(477).

- Malusis, M. A., C. D. Shackelford, and H. W. Olsen (2003), Flow and transport through clay membrane barriers, *Eng. Geol. Amsterdam*, *70*, 235–248, doi:10.1016/S0013-7952(03)00092-9.
- Melkior, T., S. Yahiaoui, D. Thoby, S. Motellier, and V. Barthes (2007), Diffusion coefficients of alkaline cations in Bure mudrock, *Phys. Chem. Earth*, *32*, 453–462.
- Meyer, K. H., and J. F. Sievers (1936), La perméabilité des membranes. I. Théorie de la perméabilité ionique, *Helv. Chim. Acta*, *19*, 649–664, doi:10.1002/hlca.19360190199.
- Mitchell, J. K. (1993), *Fundamentals of Soil Behavior*, John Wiley, New York.
- Mohajeri, A., G. A. Narsilio, P. Pivonka, and D. W. Smith (2010), Numerical estimation of effective diffusion coefficients for charged porous materials based on micro-scale analyses, *Comput. Geotech.*, *37*, 280–287, doi:10.1016/j.compgeo.2009.10.004.
- Neuzil, C. E., and A. M. Provost (2009), Recent experimental data may point out to a greater role for osmotic pressures in the subsurface, *Water Resour. Res.*, *45*, W03410, doi:10.1029/2007WR006450.
- Newman, J. S. (1991), *Electrochemical Systems*, 2nd ed., Prentice-Hall, Englewood Cliffs, N. J.
- Nguyen, V., W. Gray, G. Pinder, J. Botha, and D. Crerar (1982), A theoretical investigation on the transport of chemicals in reactive porous media, *Water Resour. Res.*, *18*(4), 1149–1156, doi:10.1029/WR018i004p01149.
- Olsen, H. W. (1960), Hydraulic flow through saturated clays, *Clays Clay Miner.*, *9*, 131–161, doi:10.1346/CCMN.1960.0090108.
- Parkhurst, D. L., and C. A. J. Appelo (1999), User's guide to PHREEQC (version 2)—A computer program for speciation, batch-reaction, one-dimensional transport, and inverse geochemical calculations, *U.S. Geol. Surv. Water Resour. Invest. Rep.*, *99-4259*, 312 pp.
- Patchett, J. G. (1975), An investigation of shale conductivity, paper presented at 16th Annual Logging Symposium, Soc. of Prof. Well Log Anal., New Orleans, La., 4–7 June.
- Pfannkuch, H. O. (1972), On the correlation of electrical conductivity properties of porous systems with viscous flow transport coefficients, in *Fundamentals of Transport Phenomena in Porous Media*, pp. 42–54, doi:10.1016/S0166-2481(08)70527-0, Elsevier, New York.
- Pride, S. R. (1994), Governing equations for the coupled electromagnetics and acoustics of porous media, *Phys. Rev. B*, *50*, 15,678–15,696, doi:10.1103/PhysRevB.50.15678.
- Prigogine, I. (1947), *Etude Thermodynamique des Phénomènes Irréversibles*, Desoer, Liège, Belgium.
- Revil, A. (1999), Ionic diffusivity, electrical conductivity, membrane and thermoelectric potentials in colloids and granular porous media: A unified model, *J. Colloid Interface Sci.*, *212*, 503–522, doi:10.1006/jcis.1998.6077.
- Revil, A. (2007), Thermodynamics of transport of ions and water in charged and deformable porous media, *J. Colloid Interface Sci.*, *307*, 254–264, doi:10.1016/j.jcis.2006.10.074.
- Revil, A., and L. M. Cathles (1999), Permeability of shaly sands, *Water Resour. Res.*, *35*(3), 651–662, doi:10.1029/98WR02700.
- Revil, A., and N. Florsch (2010), Determination of permeability from spectral induced polarization data in granular media, *Geophys. J. Int.*, *181*, 1480–1498, doi:10.1111/j.1365-246X.2010.04573.x.
- Revil, A., and A. Jardani (2010a), Stochastic inversion of permeability and dispersivities from time lapse self-potential measurements: A controlled sandbox study, *Geophys. Res. Lett.*, *37*, L11404, doi:10.1029/2010GL043257.
- Revil, A., and A. Jardani (2010b), Seismoelectric response of heavy oil reservoirs. Theory and numerical modelling, *Geophys. J. Int.*, *180*, 781–797, doi:10.1111/j.1365-246X.2009.04439.x.
- Revil, A., and P. Leroy (2004), Constitutive equations for ionic transport in porous shales, *J. Geophys. Res.*, *109*, B03208, doi:10.1029/2003JB002755.
- Revil, A., and N. Linde (2006), Chemico-electromechanical coupling in microporous media, *J. Colloid Interface Sci.*, *302*, 682–694, doi:10.1016/j.jcis.2006.06.051.
- Revil, A., M. Darot, and P. A. Pezard (1996), Influence of the electrical diffuse layer and microgeometry on the ionic diffusion coefficient in porous media, *Geophys. Res. Lett.*, *23*, 1989–1992.
- Revil, A., L. M. Cathles, S. Losh, and J. A. Nunn (1998), Electrical conductivity in shaly sands with geophysical applications, *J. Geophys. Res.*, *103*, 23,925–23,936, doi:10.1029/98JB02125.
- Revil, A., P. Leroy, and K. Titov (2005), Characterization of transport properties of argillaceous sediments: Application to the Callovo-Oxfordian argillite, *J. Geophys. Res.*, *110*, B06202, doi:10.1029/2004JB003442.
- Revil, A., C. A. Mendonça, E. Atekwana, B. Kulessa, S. S. Hubbard, and K. Bolhen (2010), Understanding biogeobatteries: Where geophysics meets microbiology, *J. Geophys. Res.*, *115*, G00G02, doi:10.1029/2009JG001065.
- Robinson, R. A., and R. H. Stokes (1965), *Electrolyte Solutions*, 2nd rev. ed., Butterworths, London.
- Rosanne, M., N. Mammari, N. Koudina, B. Prunet-Foch, J.-F. Thovert, E. Tevissen, and P. M. Adler (2003), Transport properties of compact clays. II. Diffusion, *J. Colloid Interface Sci.*, *260*, 195–203, doi:10.1016/S0021-9797(02)00240-0.
- Rousseau-Gueutin, P., J. Gonçalves, M. Cruchaudet, G. de Marsily, and S. Violette (2010), Hydraulic and chemical pulse tests in a shut-in chamber imbedded in an argillaceous formation: Numerical and experimental approaches, *Water Resour. Res.*, *46*, W08516, doi:10.1029/2008WR007371.
- Sammartino, S., A. Bouchet, D. Prêt, J. C. Pameix, and E. Tevissen (2003), Spatial distribution of porosity and minerals in clay rocks from the Callovo-Oxfordian formation (Meuse/Haute-Marne, eastern France)—Implications on ionic species diffusion and rock sorption capability, *Appl. Clay Sci.*, *23*, 157–166, doi:10.1016/S0169-1317(03)00098-X.
- Sanchez-Palencia, E. (1980), *Non-homogeneous Media and Vibration Theory*, *Lect. Notes Phys.*, vol. 127, Springer, Berlin.
- Schwartz, L. M., P. N. Sen, and D. L. Johnson (1989), Influence of rough surfaces on electrolytic conduction in porous media, *Phys. Rev. B*, *40*, 2450–2458, doi:10.1103/PhysRevB.40.2450.
- Snieder, R., S. Hubbard, M. Haney, G. Bawden, P. Hatchell, A. Revil, and the DOE Geophysical Monitoring Working Group (2007), Advanced noninvasive geophysical monitoring techniques, *Annu. Rev. Earth Planet. Sci.*, *35*, 653–683, doi:10.1146/annurev.earth.35.092006.145050.
- Stingaciu, L. R., L. Weiermüller, S. Haber-Pohlmeier, S. Stapf, H. Vereecken, and A. Pohlmeier (2010), Determination of pore size distribution and hydraulic properties using nuclear magnetic resonance relaxometry: A comparative study of laboratory methods, *Water Resour. Res.*, *46*, W11510, doi:10.1029/2009WR008686.
- Teorell, T. (1935), An attempt to formulate a quantitative theory of membrane permeability, *Proc. Soc. Exp. Biol. Med.*, *33*, 282–285.
- Tournassat, C., Y. Chapron, P. Leroy, M. Bizi, and F. Boulahya (2009), Comparison of molecular dynamics simulations with triple layer and modified Gouy-Chapman models in 0.1 M NaCl-montmorillonite system, *J. Colloid Interface Sci.*, *339*, 533–541, doi:10.1016/j.jcis.2009.06.051.
- van't Hoff, J. H. (1888), The function of osmotic pressure in the analogy between solutions and gases, *Philos. Mag., Ser. 5*, *26*(159), 81–105.
- Vaudelet, P., A. Revil, M. Schmutz, M. Franceschi, and P. Bégassat (2011), Induced polarization signatures of cations exhibiting differential sorption behaviors in saturated sands, *Water Resour. Res.*, *47*, W02526, doi:10.1029/2010WR009310.
- Wang, M., and A. Revil (2010), Electrochemical charge of silica surface at high ionic strength in narrow channels, *J. Colloid Interface Sci.*, *343*, 381–386, doi:10.1016/j.jcis.2009.11.039.
- Waxman, M. H., and L. J. M. Smits (1968), Electrical conductivities in oil bearing shaly sands, *Soc. Pet. Eng. J.*, *8*, 107–122, doi:10.2118/1863-A.
- Westermann-Clark, G. B., and C. C. Christoforou (1986), The exclusion-diffusion potential in charged porous membranes, *J. Electroanal. Chem.*, *198*(2), 213–231, doi:10.1016/0022-0728(86)90001-X.
- Whitaker, S. (1967), Diffusion and dispersion in porous media, *AIChE J.*, *13*(3), 420–427.
- Yven, B., S. Sammartino, Y. Géraud, F. Homand, and F. Villeras (2006), Mineralogy, texture and porosity of Callovo-Oxfordian argillites of the Meuse/Haute-Marne region (eastern Paris basin), *Mem. Soc. Geol. Fr.*, *178*, 73–90.
- Zukoski, C. F., and D. A. Saville (1986a), The interpretation of electrokinetic measurements using a dynamic model of the Stern layer. I. The dynamic model, *J. Colloid Interface Sci.*, *114*, 32–44, doi:10.1016/0021-9797(86)90238-9.
- Zukoski, C. F., and D. A. Saville (1986b), The interpretation of electrokinetic measurements using a dynamic model of the Stern layer. II. Comparisons between theory and experiments, *J. Colloid Interface Sci.*, *114*, 45–53, doi:10.1016/0021-9797(86)90239-0.

N. Lu, Division of Engineering, Colorado School of Mines, Golden, CO 80401, USA.

A. Revil and W. F. Woodruff, Department of Geophysics, Colorado School of Mines, Green Center, 1500 Illinois St., Golden, CO 80401, USA. (arevil@mines.edu)